Synthesis and characterization of novel proton-conductive composite membranes derived from the hybridization of metal oxyhydroxide nanoparticles and organic polymers for fuel cell applications

by

Liwei Zhang

Department of Civil and Environmental Engineering
Duke University

Date: 03/22/2010
Approved:

_____
Mark Wiesner, Supervisor

_____
Marc Deshusses

_____
Heileen Hsu-Kim

Thesis submitted in partial fulfillment of
the requirements for the degree of Master of Science in the Department of
Civil and Environmental Engineering in the Graduate School
of Duke University

2010

ABSTRACT

Synthesis and characterization of novel proton-conductive composite membranes derived from the hybridization of metal oxyhydroxide nanoparticles and organic polymers for fuel cell applications

by

Liwei Zhang

Department of Civil and Environmental Engineering
Duke University

Date: 03/22/2010
Approved:

_____
Mark Wiesner, Supervisor

_____
Marc Deshusses

_____
Heileen Hsu-Kim

An abstract of a thesis submitted in partial
fulfillment of the requirements for the degree
of Master of Science in the Department of
Civil and Environmental Engineering in the Graduate School
of Duke University

2010

Abstract

A fuel cell is a device that converts chemical energy directly to electricity. Fuel cells have high energy conversion efficiencies with potentially less release of environmental pollutants. Therefore, they are regarded as a promising technique to address future energy needs. The proton exchange membrane (PEM) is one of the fundamental parts in fuel cell system and the synthesis of novel PEMs is an active area of research. In this work, several metal oxyhydroxide (FeOOH and CoOOH) + organic polymers (polyvinyl alcohol and polysulfone) composite proton exchange membranes are synthesized and their proton conductivities, surface properties, spatial structures and mechanical strength are investigated by Electrochemical Impedance Spectroscopy (EIS), Attenuated total reflectance-Fourier transform infrared (ATR-FTIR) spectroscopy, scanning electron microscope (SEM) and tensile resistance measurement.

Experimental results of EIS reveal that the protonic conductivities of PVA membrane filled with FeOOH treated by sonication were high at moderate and high RHs (6.54×10^{-3} S/cm at 81% RH and 0.0106 S/cm at 97% RH), and are perhaps comparable to those of Nafion measured by the same method (1.87×10^{-3} S/cm at 81% RH and 4.26×10^{-3} S/cm at 97% RH). A PVA membrane filled with FeOOH treated only by acetic acid had lower protonic conductivities (1.33×10^{-3} S/cm at 81% RH and 3.18×10^{-3} S/cm at 97% RH) compared with the PVA membrane filled with sonication-treated

FeOOH at moderate and high RHs. All cobalt-filled PVA membranes had lower protonic conductivities than iron-filled PVA membranes. The protonic conductivities of FeOOH-PVA and CoOOH-PVA composite membranes were close to those of corresponding FeOOH and CoOOH nanoparticles at high RHs, but the protonic conductivities of composite membranes dropped considerably as RH values decreased (<60%). FeOOH-polysulfone and CoOOH-polysulfone composite membranes exhibited low protonic conductivities at all RHs (most conductivity values were below 10^{-5} S/cm), suggesting that polysulfone is not an ideal material for support of proton-conductive metal oxyhydroxides.

Experimental results of ATR-FTIR suggest that the reaction with acetic acid can lead to a decrease of hydroxyl groups on the surface of FeOOH nanoparticles, as evidenced by the fact that the protonic conductivities of samples treated by acetic acid only were lower than those of samples treated by sonication. The spectrum of FeOOH (sonication) + PVA composite membrane displayed the characteristic absorption band of FeOOH very clearly, which implies that a high percentage of FeOOH is distributed on the surface of the composite membrane. However, there were no significant differences between the spectra of pure PVA and CoOOH (sonication) + PVA, which means that there are few CoOOH nanoparticles distributed on the surface of the composite membrane. Similarly, no significant differences between the spectra of pure polysulfone and polysulfone + metal oxyhydroxide composites were observed. These results suggest

that the percentage of metal oxyhydroxide particles that are distributed on the surface of the composite is low, and is consistent with the fact that the polysulfone-based composite membranes had very low protonic conductivities at all RHs.

The SEM images of ferroxane (carboxylate FeOOH) + PVA composites revealed that there was significant aggregation among ferroxane nanoparticles in the composite, which results in a decrease of specific surface area of ferroxane and a drop of protonic conductivity of the composite at low RHs.

The tensile force resistance of the ferroxane-PVA composite membrane was tested and the stress-strain curve of the membrane was obtained, which showed that the composite membrane had a higher tensile force resistance than the Nafion membrane. A higher content of ferroxane in the ferroxane-PVA composite membrane resulted in a stronger tensile resistance. Though the increase of ferroxane in the composite also resulted in a decrease in elasticity, the elasticity of the composite membrane with highest ferroxane content ($\varepsilon_B = 0.381$) was still comparable to that of Nafion membrane ($\varepsilon_B = 0.417$). In summary, the ferroxane + PVA composite membrane had better mechanical properties than Nafion.

Based on the findings achieved in this paper, it would appear that the FeOOH + PVA composite membranes are like Nafion, limited with respect to low protonic conductivities at low RHs. To overcome this drawback, several possible approaches are proposed, including the exploration of selection methodology for quick pick-up of

polymers that can work well at low RHs, prevention of nanoparticles from aggregation during the preparation process, exploration of new metal oxyhydroxide nanoparticles that may possess high protonic conductivity at low RHs and synthesis of composite membrane that can endure high-temperature sintering.

Dedication

The results obtained in the experiments of EIS, ATR-FTIR, SEM and tensile force measurement in this research present useful information on the proton conductivities, surface and structural characteristics and mechanical properties of the composite PEM samples. The information is instructive and helpful for researchers to synthesize new composite PEMs or make further improvements on composite PEMs that have been synthesized, so as to make the composite PEMs more competitive to get applied in commercial PEMFC systems. The fuel cells installed with novel composite PEMs may get applied in a wide range of applications, including automobiles, potable electronic devices and even spaceships.

Contents

List of Tables

List of Figures

Acknowledgements

I would like to express my sincere gratitude to my advisor--Dr. Wiesner. His innovative ideas, rigorous attitude to do research work and valuable recommendations on my research have nurtured and benefited me greatly. Without his supervision, it is impossible for me to finish my research work and compose this thesis.

I would like to thank Dr. Deshusses for allowing me to do experiments in his lab and giving me valuable suggestions on the improvement of experimental methods and appropriate manners to make presentations. I would also like to thank Dr. Hsu-Kim for her suggestions and revisions on my thesis.

Last but not least, I would like to thank all my friends and my family for their continuous support on my research. Their help, care and encouragement enable me to finish my research and enjoy a vivid and happy life in the United States.

1. Background

1.1 Introduction to fuel cells

A fuel cell (FC) can be defined as an electrochemical "device" that continuously converts chemical energy to electric energy (and some heat) as long as fuel and oxidant are supplied [1]. Fuel cell technology has been regarded as a promising solution to some grand challenges (such as energy shortages and environmental pollution) that have threatened the life of human beings, because fuel cells can be operated without release of pollutants (the final product is water if hydrogen is applied as the fuel) and fuel cell systems have both high output energy density and energy conversion efficiency [2-4]

1.1.1 History of fuel cells

The development history of fuel cells can be traced back to the 19th century, when William Grove developed the so-called "gaseous voltaic battery", which used hydrogen and oxygen as reactants and platinum as electrodes [1]. In 1937, Baur and Preis [1] developed the solid oxide fuel cell, which was operated at high temperature (1050 ℃) using a mixture of ZrO_2 and Y_2O_3 as the electrolyte. In 1959, GE Corporation made the first attempt to develop polymer electrolyte membrane fuel cells. They prepared phenolic polymer membranes by polymerization of phenol–sulfonic acid with formaldehyde and tested the performance of these membranes in fuel cell systems. Unfortunately, these membranes had low mechanical strength and a short

lifetime of 300–1000h and showed a relatively low power density [5]. In the 1970s, Du Pont made a breakthrough to develop a perfluorosulfonic acid-based membrane called "Nafion", which doubled the maximum proton conductivity and extended the lifetime to 10^4--10^5h [2]. The Nafion membrane was quickly applied in fuel cell systems and helped fuel cells to establish a competitive role in the market. Fuel cells have had a wide range of applications now and their sizes can vary from 200 Kw power stations to power separate buildings to 100 mW mini power generators that can add baseload capacity to certain electric utilities [6]. The most promising application of fuel cells is Fuel Cell Electric Vehicle (FCEV) [4], such as Chevrolet Equinox of GM and Focus FCEV of Ford.

1.1.2. Principle of fuel cells

The electricity--generation processes of all types of fuel cells involve the transfer of ions (either from fuels or oxidants) through the electrolyte between anode and cathode and the release of electrons from fuels to external circuit. Figure 1 explains how a fuel cell works, with the use of widely applied hydrogen/oxygen polymer electrolyte membrane fuel cell (PEMFC) as an example. On the anode side, hydrogen diffuses to the anode catalyst layer where it later dissociates into protons and electrons. The protons are conducted through the proton exchange membrane (electrolyte) to the cathode, but the electrons are forced to travel in an external circuit, because the proton exchange membrane is electrically insulating. On the cathode side, oxygen molecules

react with the electrons (which have traveled through the external circuit and generated electrical power) and protons to form water.

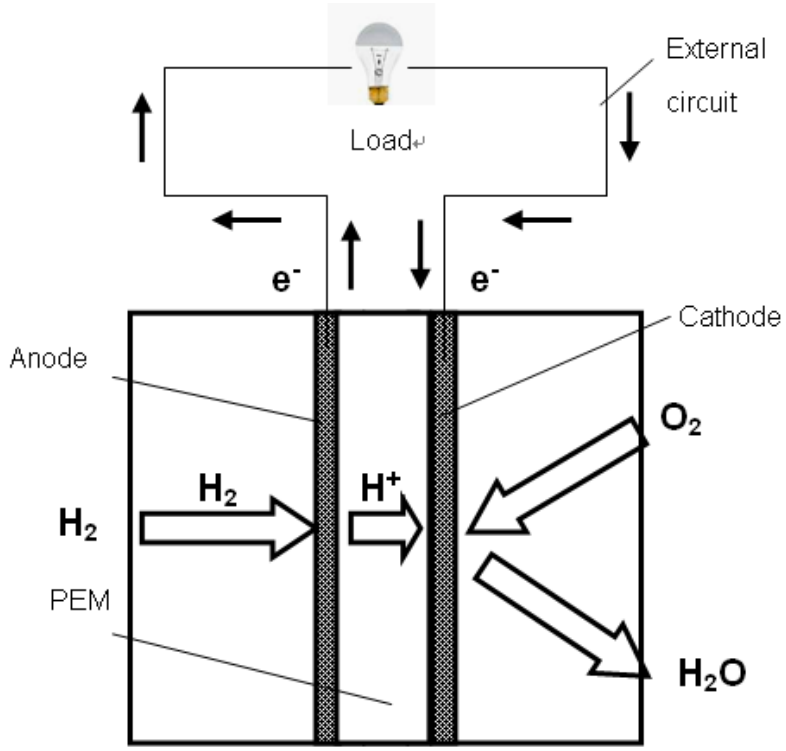

Figure 1: Schematic view of a proton exchange membrane fuel cell (PEMFC)

1.1.3. Classification of fuel cells

In general, fuel cells can be classified based on the variation of ions traveling through the electrolyte. Figure 2 shows the five main categories of fuel cells. A solid oxide fuel cell (SOFC) is composed of two porous electrodes and a solid oxide ceramic electrolyte is "sandwiched" between the electrodes [4]. SOFCs work at very high operation temperatures, thus no catalyst layers are needed on the electrode surfaces [4]. A molten-carbonate fuel cell (MCFC) employs an electrolyte that is composed of a

mixture of alkali metal carbonates. The fuel cell is operated well above the melting point of the carbonates, and the carbonate ion (CO_3^{2-}) was found to be the charge transport mediators within the molten electrolyte [7]. A phosphoric acid fuel cell (PAFC) applies liquid-form phosphoric acid as the electrolyte to transfer charge mediators (H^+). This system can only work at relatively high temperatures (around 200 ℃), because phosphoric acid solidifies at lower temperatures. Furthermore, the dissolution of air-cathode catalysts in hot phosphoric acid under PAFC operating conditions is a significant problem that limits its applicability [8]. An alkaline fuel cell (AFC) uses potassium hydroxide in aqueous solution as the electrolyte. The AFC is the first fuel cell type applied in practical services and it has been proven to possess high power densities and long lifetimes in certain applications, such as space shuttles [9]. However, the AFC system is easily poisoned, because the carbon dioxide can react with the hydroxide ion present in the electrolyte to form carbonate (CO_3^{2-}), thereby reducing the hydroxide ion concentration in the electrolyte and subsequently deteriorating the overall efficiency of the fuel cell [9]. As a result, researchers gradually lost interest in the AFC, which is being replaced by polymer electrolyte membrane fuel cells (PEMFCs). Polymer electrolyte membrane fuel cells (PEMFCs) are the most widely used fuel cell system now, because they are compact, have a relatively long operation life time, offer quick start-up, and can be operated at low temperatures [3]. They are best suited for applications where a quick start-up and a benign operation

environment are required, such as in automobiles. Table 1 summarizes the characteristics of different types of fuel cells.

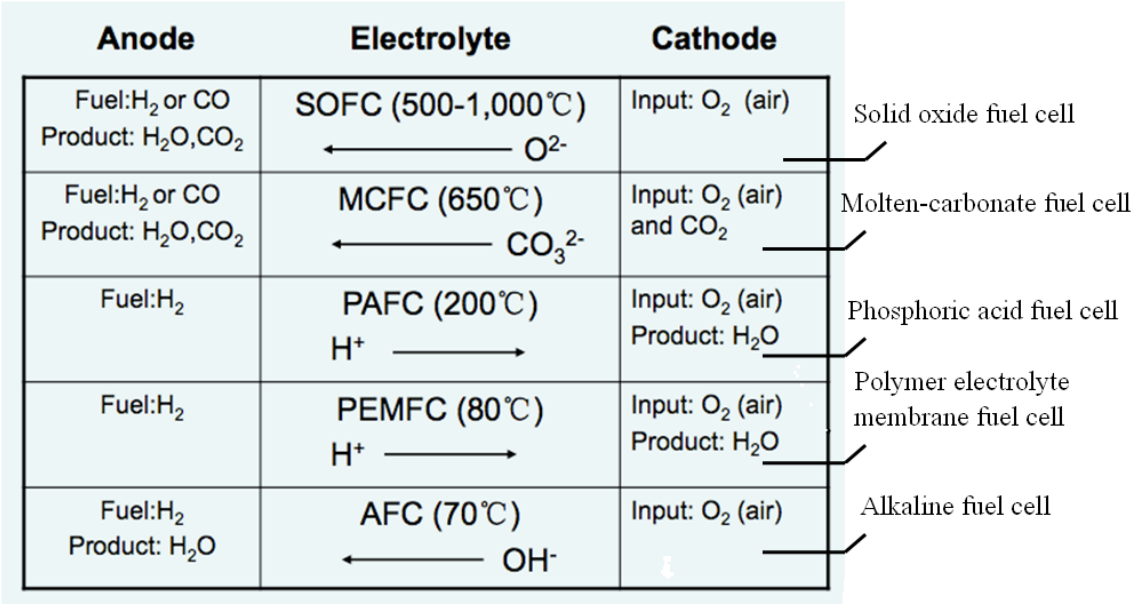

Figure 2: Classification of fuel cells (modified from [10])

Table 1: Characteristics of fuel cells [3]

Types of fuel cells	Typical operating temperature (℃)	Efficiency (%)	Applications			
			Power for household appliances	Power in small scale	Power cogeneration in large scale	Vehicles
SOFC	800-1000	50-60	Yes	Yes	Yes	No
MCFC	600-650	50-60	No	Yes	Yes	No
PAFC	175-220	40-45	No	Yes	No	No
PEMFC	50-120	40-50	Yes	Yes	No	Yes
AFC	50-90	50-70	Yes	Yes	No	Yes

1.2 Fundamentals of proton exchange membranes (PEMs)

The proton exchange membrane is one of the fundamental parts of PEMFC system, because it connects the anode and cathode and its failure will cause the whole system to become inoperable. Furthermore, the PEM must possess properties that make it compatible with the environments in both the anode and cathode chambers, which is a requirement difficult to meet. Therefore, the synthesis and characterization of proton exchange membrane is one of the most frontier areas in fuel cell research.

1.2.1. Definition and principle of PEMs

The PEM (proton exchange membrane) is a thin membrane that separates the anode and cathode in a fuel cell and acts both as a proton-conducting medium and a barrier to avoid direct contact between the fuel and oxidant [3]. A proton exchange membrane needs to have specific properties that enable it to work well in fuel cells: *i*) High proton conductivity to support high currents with minimal resistive losses and zero electronic conductivity; *ii*) Adequate mechanical strength and stability; *iii*) Chemical and electrochemical stability under operating conditions; *iv*) extremely low fuel or oxidant by-pass to maximize columbic efficiency; *v*) Low water transport through diffusion and *vi*) electro-osmosis and capability for fabrication into membrane electrode assemblies [3, 11].

The PEM contains many proton-conductive functional groups, which allows protons to transfer from one group to another. These groups can constitute a channel

which provides protons the access to travel across the membrane. Figure 3 shows a schematic polymer PEM structure, which displays how the protons are transferred. Figure 4 displays the schematic diagram of water channels that present in the inner structure of Nafion, which explains how protons travel across the Nafion membrane.

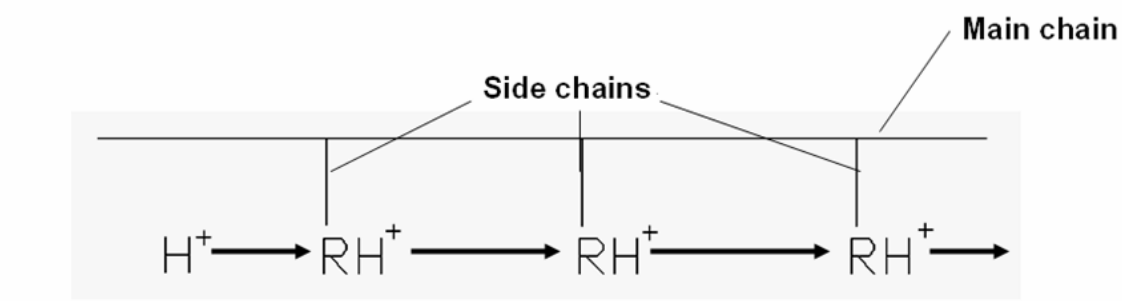

Figure 3: Polymer PEM structure. Proton-conductive groups (R) are fixed to polymeric chains, but protons are free to migrate from one group to another. One proton will collide with one proton-conductive group, resulting in the detachment of the proton originally attached with the group. The proton detached will become free and collide with the next group.

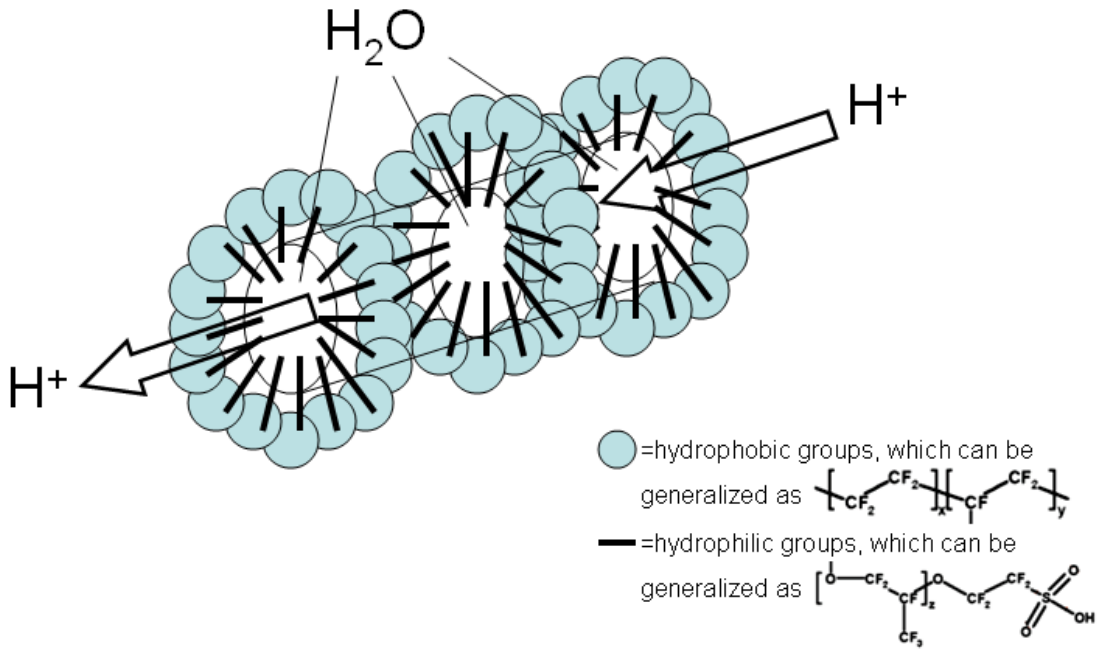

Figure 4: Water channels in the intrinsic structure of Nafion. The figure is drawn based on the water channel model developed by Schmidt-Rohr and Chen in 2008 [12]. The tail-like hydrophilic groups can attract a large amount of water molecules by sulfonic groups in their ends. The water molecules cluster together and form channels for protons to go through.

1.2.2. Classification of PEMs

After decades of development, there have been hundreds of institutions that are focusing on the development of PEMs around the world and the specific categories of PEMs that have been synthesized by these institutions are extremely vivid. In general, the PEMs can be classified into three main categories: polymeric PEM, ceramic PEM and inorganic-organic composite PEM (figure 5).

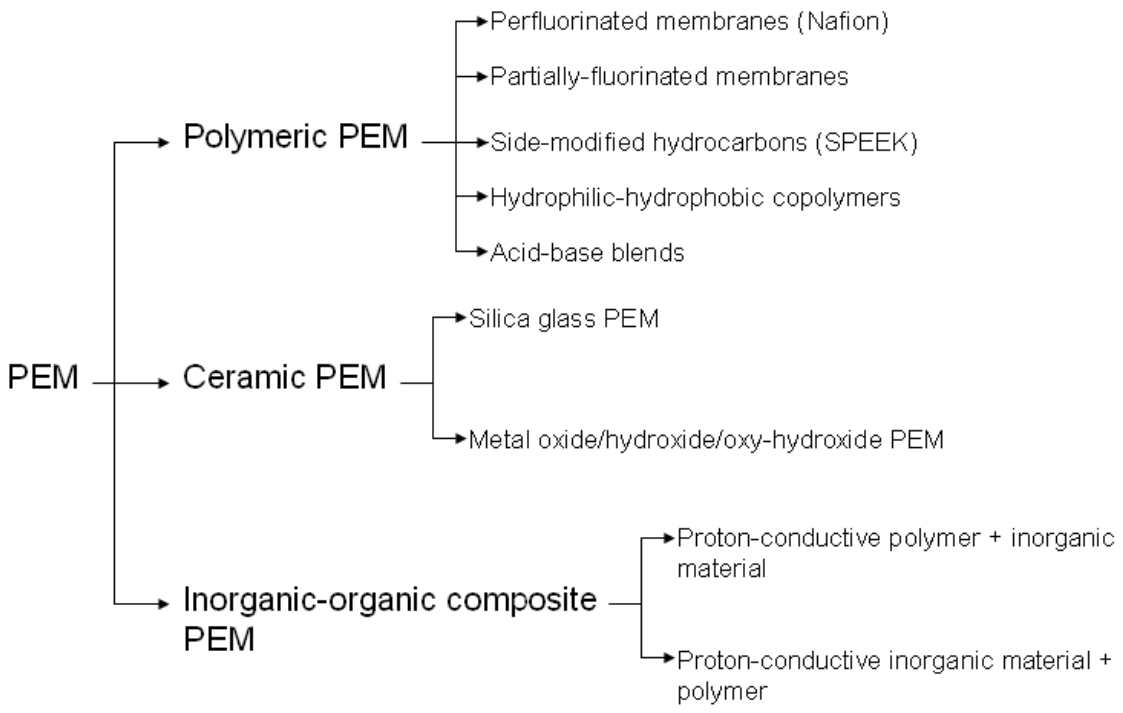

Figure 5: Classification of PEMs

Though researchers have developed a large number of different types of PEMs, only a few of them are commercially available to customers and Nafion membrane is the most widely used PEM among them. Nafion membrane was invented by researchers at DuPont in the early 1970s and it has brought a large profit to DuPont since it was invented. The membrane has a perfluorinated polymeric structure, with -attached sulfonic acid groups that act as proton-conductive groups. The protonic conductivity of Nafion membrane is strongly dependent on water content and temperature. A study shows that for a fully hydrated membrane (water content=22, represented by the number of absorbed water molecules per sulfonic acid group), the protonic conductivity is about 0.1 S cm^{-1} at room temperature. If water content

decreases to 14, the protonic conductivity decreases to 0.06 S/cm [13]. As to temperature, protonic conductivity increases significantly with temperature increase at a range from room temperature to 80℃. At 80℃, the protonic conductivity of a fully hydrated Nafion membrane can reach 0.18 S/cm [4]. Nafion membranes possess many of the desired properties that enable it to be a good candidate for FC systems. The desired properties include high proton conductivity at normal conditions, excellent chemical and mechanical stability and low permeability of both fuel and oxidant [3, 14-16]. However, there are some intrinsic drawbacks of Nafion that make Nafion fail to become a perfect candidate for FC applications. For example, the upper operation temperature limit of Nafion is low (only 80-120℃), because Nafion will dehydrate (thus lose proton conductivity) when the temperature exceeds 80 ℃ and a significant drop of proton conductivity can be observed at 120℃ [17]. The proton-conductive performance of Nafion also becomes bad at low relative humidity [18]. Moreover, Nafion has relatively high methanol permeability [19-21], which drastically deteriorates the performance of direct methanol fuel cells that use Nafion as PEMs. Therefore, to develop alternatives of Nafion that can overcome the drawbacks of Nafion and get applied in conditions that are not suitable for Nafion is quite necessary.

1.3 Introduction to ceramic PEMs derived from iron oxyhydroxide

Over recent decades, researchers have a growing interest in testing the performance of ceramic materials as possible alternatives of Nafion for fuel cell

applications [18, 22, 23] and ceramic PEMs derived from iron oxyhydroxide have shown great potential to substitute Nafion in certain operation conditions [18, 24]. The advantages of the ceramic membrane derived from iron oxyhydroxide include: excellent thermal and chemical stability, which enables the membrane to be used at very high temperature; Low material cost and high proton conductivity at low relative humidities [18]. Previous works have shown that the ceramic membrane derived from ferroxane (carboxylate-FeOOH) nanoparticles sintered at 300℃ has a proton conductivity of 2.21×10^{-2} S/cm at 58%RH and 2.65×10^{-2} S/cm at 100%RH, which is higher than that of Nafion (1.6×10^{-3} S/cm at 58%RH and 1.30×10^{-2} S/cm at 100%RH), especially when the RH is low [18, 24]. Moreover, the ferroxane ceramic membrane is a good candidate for applications to direct methanol fuel cells (DMFCs), because normal Nafion can not meet the low methanol permeability requirement for DMFCs and the ferroxane membrane has an extremely low methanol permeability (84% less than that of Nafion) [18, 25]

The proton is conducted by two main pathways in the ceramic membrane derived from iron oxyhydroxide: *i*) conduction by hydroxyl groups on the surface of the material; *ii*) conduction by adsorbed water on the surface of the material. At low humidity, there is little or no physisorbed water on the surface of the membrane and protons are mainly conducted by the chemisorbed hydroxyl layer (pathway *i*). To be specific, protons will "hop" onto the adjacent hydroxyl group by hydroxyl dissociation

[26, 27]. The chemisorbed hydroxyl group layer is unaffected by subsequent changes in relative humidity, but it can be removed thermally at high temperature [18]. At high humidity, a complete physisorbed water layer will cover the surface of the material and protons will be conducted mainly by the physisorbed water layer (pathway *ii*). Specifically, a free proton combines with a water molecule first to form a H_3O^+. The H_3O^+ then releases the proton to a nearby H_2O molecule at the physisorbed water layer and ionizes it to produce another H_3O^+ molecule in a process referred as a Grotthuss chain reaction [18, 28-30] (figure 6).

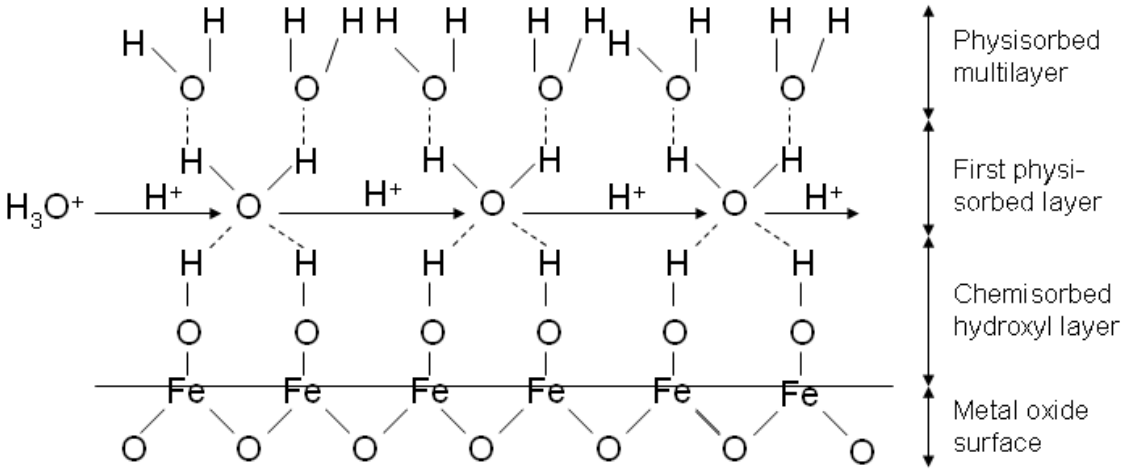

Figure 6: Schematic diagram of Grotthuss chain reaction (modified from the figure in [18])

The crystal structure of iron oxyhydroxide favors the adsorption of water molecules inside the crystal and the Grotthuss chain reaction is easy to be conducted inside the crystal. Figure 7 shows the spatial structure of iron oxyhydroxide crystal and a side view of the crystal. Iron oxyhydroxide crystal is composed of layers of

oxohydroxo octahedra with oxygen atoms as vertexes and Fe atoms occupy the octahedral interstices inside the octahedra [31]. The layers of octahedra are partially separated from each other and hydrogen bonds are the sole connections between these layers. The spaces between octahedron layers are quite large and water molecules can occupy the spaces to form channels to transfer protons, which are similar to the water channels formed inside the Nafion membrane.

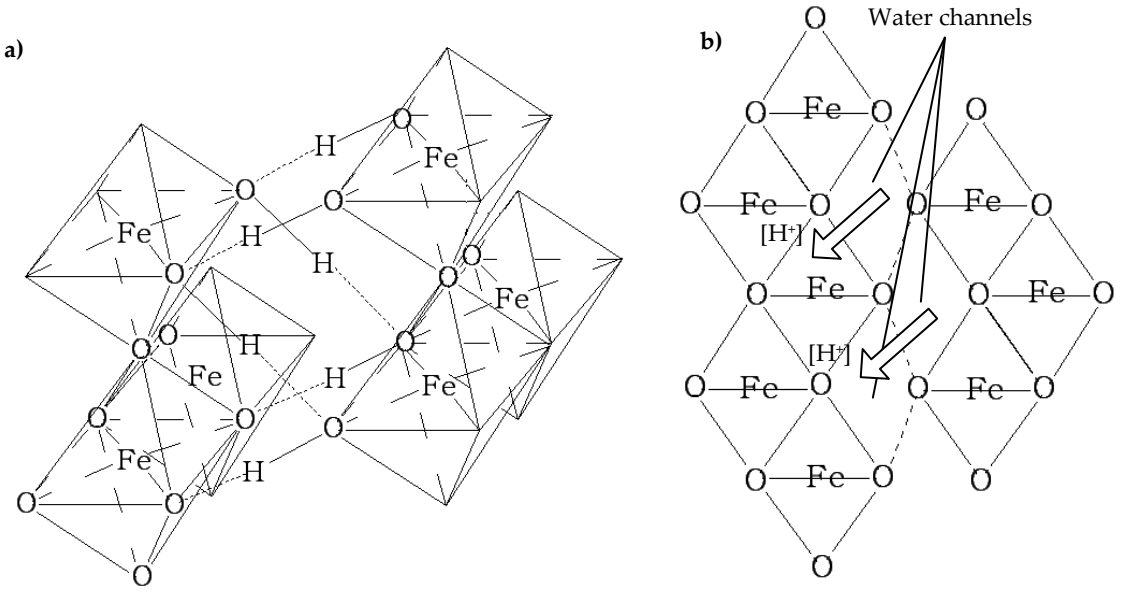

Figure 7: Spatial structure of FeOOH crystal (a) and a projection view of the crystal (b) (The figure was drawn based on contents in [31] and [32]). Hydrogen bonds are shown in dashed lines between hydrogen atoms and oxygen atoms. Spaces between layers of octahedrons allow water molecules to form water channels to conduct protons.

The sol-gel process is the traditional approach to prepare ceramic thin films with nano-sized pores [18]. However, for the FeOOH ceramics, the commonly-used preparation method is to make coarse FeOOH particles (lepidocrocite) react with

carboxylic acid to form nano-sized ferroxane (carboxylate-FeOOH) ceramics. One drawback of the ferroxane ceramic membrane is that the proton conductivity becomes low at low RHs, due to the residual of acetic acid groups. To be specific, the particle size of raw material (lepidocrocite) is greatly reduced in the preparation process (reaction with acetic acid), but the use of acetic acid will introduce acetic acid groups to the surface of the material. When the acetic acid groups are present, the transfer of protons among physisorbed water molecules is hindered and the increase of proton conductivity is restricted. To remove acetic acid groups from the surface of the ceramic membrane, a sintering process is needed. After sintering the membrane at a high temperature (300℃) for several hours, the proton conductivity of the membrane increases due to the removal of acetic acid [18]. A brief summary of the synthesis processes of the ferroxane membrane is shown in figure 8.

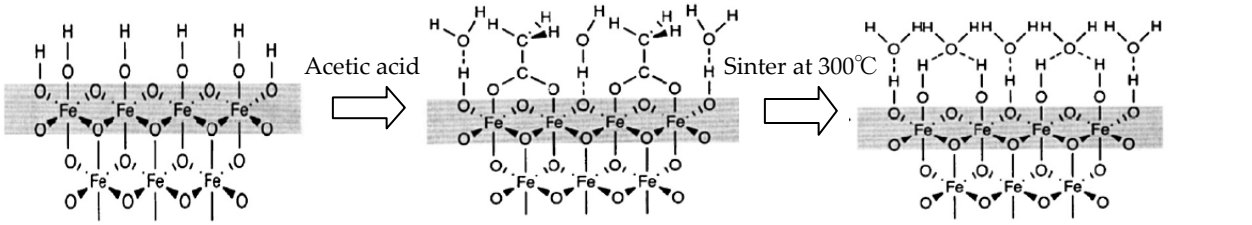

Figure 8: Ferroxane ceramic membrane preparation processes (modified from [18])

The main bottleneck that hinders iron oxyhydroxide ceramic membranes to be applied in real fuel cell systems is their poor ductility and compression resistance. Iron oxyhydroxide ceramic membranes are quite brittle and can be easily broken to very small pieces, because the precursor of those membranes--lepidocrocite has very poor mechanical properties. Compared with other common materials, the hardness of lepidocrocite is very low (5 Gpa), while Al_2O_3 is 20.6 Gpa and α-SiO_2 is 30.6 Gpa [33, 34]. The brittleness of lepidocrocite can be interpreted in the aspect of its crystal structure. As mentioned earlier, the crystal of lepidocrocite is composed of many layers of oxohydroxo octahedrons and hydrogen bonds are the main connections to hold these layers together. Because the hydrogen bonds are relatively weak and can not provide strong attractions between layers, the crystal is easy to get cleaved parallel to the layers [32]. Therefore, it is difficult to synthesize iron oxyhydroxide ceramic membranes with desired mechanical properties that meet the requirements to get applied in PEMFCs. Moreover, if organic fuel is applied at anode side (e.g., methanol), some molecules of the fuel may get adsorbed on the surface of the iron oxyhydroxide ceramic membrane and that can cause a decrease of proton conductivity of the membrane [35].

1.4 Introduction to inorganic-organic hybrid materials and the feasibility to incorporate organic polymers with metal oxyhydroxide materials

Hybrid material (or composite material) can be defined as a material that includes two or more blended compounds on the molecular scale. In most cases, at least one of those compounds is inorganic and at least one is organic [33]. Though inorganic and organic materials were first combined long ago, in-depth studies on composite materials began at the end of the 20th century, with the help of novel physico-chemical characterization methods [33]. The studies on composite materials have drawn great attention recently, because inorganic-organic components can combine dissimilar properties of inorganic and organic materials, and the components can exhibit the desired properties of both material types [33]. The incorporation of inorganic nanoparticles with special properties in organic polymers to create multifunctional groups is one example [33], while another is the surface modification of plastics with hard poly(methylsiloxane)s to increase the abrasion resistance of plastics [36].

Inorganic-organic nanocomposite is a special group of hybrid materials that possesses a structural unit (either the inorganic or the organic) with a size ranged between 1 and 100 nm [33]. The nano-scale structural units in the nanocomposites are usually inorganic materials and these inorganic units are usually discrete. Examples of

the discrete inorganic units include metal and metal derivatives, silica-based crystals and carbon-based nanomaterials (nanorods, fullerene and nanotubes) [37] [38] [39].

As mentioned above, the approach to fill organic polymers with inorganic nano-scale materials has become a commonly-used technique and the incorporation of organic polymers with inorganic materials combines the desired properties of organic polymers and inorganic materials together. Therefore, to combine the iron oxyhydroxide nanoparticles with high proton conductivity and organic polymers with high mechanical strength may yield a composite material that possesses both high proton conductivity and high mechanical strength and this material may be a promising candidate to be applied in real fuel cell systems. A polymer that is suitable for the synthesis of inorganic-organic composite membrane needs to meet several basic criteria. Firstly, the polymer needs to have high mechanical strength; secondly, the polymer needs to have surface properties that favor a high distribution of inorganic nanoparticles on its surface; thirdly, the polymer needs to have traversed channels open for the occupation of proton-conductive inorganic nanoparticles. There have been a few studies that focus on the combination of proton-conductive inorganic materials and organic polymers to fabricate proton-conductive membranes. Kim, et al tried to incorporate sulfonated poly(arylene ether sulfone) with PTA ($H_3PW_{12}O_{40}{\cdot}nH_2O$) and the composite membrane synthesized showed a proton conductivity up to 0.15 S/cm at a temperature range of 100-130℃, which is much

higher than that of pure Nafion at the given temperature range [40]. Genova-Dimitrova, et al filled sulfonated polysulfone with 8% of phosphatoantimonic acid ($H_nSb_nP_2O_{3n+5} \cdot xH_2O$, ($n$ = 1 and 3)) and this composite membrane has a proton conductivity of 0.06 S cm^{-1} at 80℃ and 98% of relative humidity (RH), which is comparable to the conductivity of Nafion [41]. However, all the inorganic materials tested in these studies are inorganic complex acids and the research work shown in my paper is the first attempt to combine metal oxyhydroxide materials with organic polymers to produce proton exchange membranes. Therefore, my thesis can be instructive to researchers who are focusing on the development of novel inorganic-organic composite proton exchange membranes.

2. Objectives and hypothesis

2.1 Objectives

The goal of my research is to synthesize and characterize proton-conductive composite membranes derived from the combination of metal oxyhydroxide nanoparticles and organic polymers. My specific aims include: 1) Combine FeOOH-derived nanoparticles with various polymers, such as polyvinyl alcohol (PVA) and polysulfone and test the proton conductivities of the products at different humidities; 2) Characterize the structures, chemical compositions and mechanical properties of these composite membranes with the use of FTIR, SEM and the tensile tester; 3) Investigate the feasibility to use alternative metal oxyhydroxide nanoparticles (CoOOH) in the composite membranes instead of iron oxyhydroxide and 4) Investigate the feasibility to utilize sonication instead of acetic acid to reduce the size of iron oxyhydroxide and cobalt oxyhydroxide particles.

2.2 Hypothesis

My research is based on the hypothesis that the proton exchange membrane produced via the combination of proton-conductive inorganic nanoparticles and organic polymers can possess both the high proton conductivity of inorganic nanoparticles and excellent mechanical strength of organic polymers.

3. Materials and methods

3.1 Preparation of materials

3.1.1 Preparation of lepidocrocite (FeOOH)

To prepare for lepidocrocite which is the precursor of iron-based nanoparticles, 500 mL of 0.2 mol/L NaOH (Sigma-Aldrich Inc., St. Louis, MO) was mixed with 500 mL of 0.12 mol/L $FeCl_2{\cdot}4H_2O$ (MP Biochemicals, Solon, OH) to produce lepidocrocite. The [$FeCl_2{\cdot}4H_2O$]/[NaOH] ratio was kept at 0.6 because the ratio was reported as favorable for pure lepidocrocite formation [42]. Then the mixture was thoroughly aerated with an air bubble stone and stirred for 12 hours with the use of a magnetic stirrer plate (Fisher Scientific, Pittsburgh, PA), in order to completely oxidize $FeCl_2{\cdot}4H_2O$ to lepidocrocite. The resultant was then dried out in the oven (Fisher Scientific, Pittsburgh, PA) at 80℃ to get lepidocrocite particles.

3.1.2 Preparation of iron-based nanoparticles

Two different approaches were adopted to reduce the particle size of coarse lepidocrocite to nano-scale lepidocrocite. One approach was to get the lepidocrocite reacted with acetic acid and this reaction can yield nano-scale ferroxane (carboxylate-FeOOH) particles [18, 43]. Lepidocrocite particles were dissolved in double deionized (DDI) water and got reacted with pure acetic acid (EMD Chemicals, Gibbstown, NJ) at a [Fe/AA] ratio of 1.5:1. The solution was stirred at room temperature over night and centrifuged at 26832 xg RCF for 2 hours with the use of a 5804R centrifuge machine

(Eppendorf North America, Hauppauge, NY) to remove coarse particles. The supernatant after centrifugation was dried out at 80 ℃ to get pure ferroxane nanoparticles. The other approach was to apply sonication to reduce the size of lepidocrocite particles. 0.5g lepidocrocite particles were suspended in 20 mL of DDI water and the sonication probe of the ultrasonic liquid processor (Misonix Inc., Farmingdale, NY) was immersed into the suspension. To avoid the interference of temperature increase during the sonication process, ice pieces were put around the beaker containing the suspension. Total sonication time was 1 hour, with sonication amplitude of 70. After sonication, the suspension was centrifuged at 26832 xg RCF for 2 hours to remove coarse particles. Then the supernatant was dried out at 80 ℃ to get pure lepidocrocite nanoparticles.

3.1.3 Preparation of cobalt-based nanoparticles

Ceramic membranes derived from cobalt oxyhydroxides may possess proton-conductive property that is similar to iron-based ceramic membranes, because the crystal structure of cobalt oxyhydroxide is similar to that of iron oxyhydroxide (figure 9). The crystal of cobalt oxyhydroxide is also composed of layers of octahedrons and spaces between layers of octahedrons allow the occupation of water molecules to conduct protons.

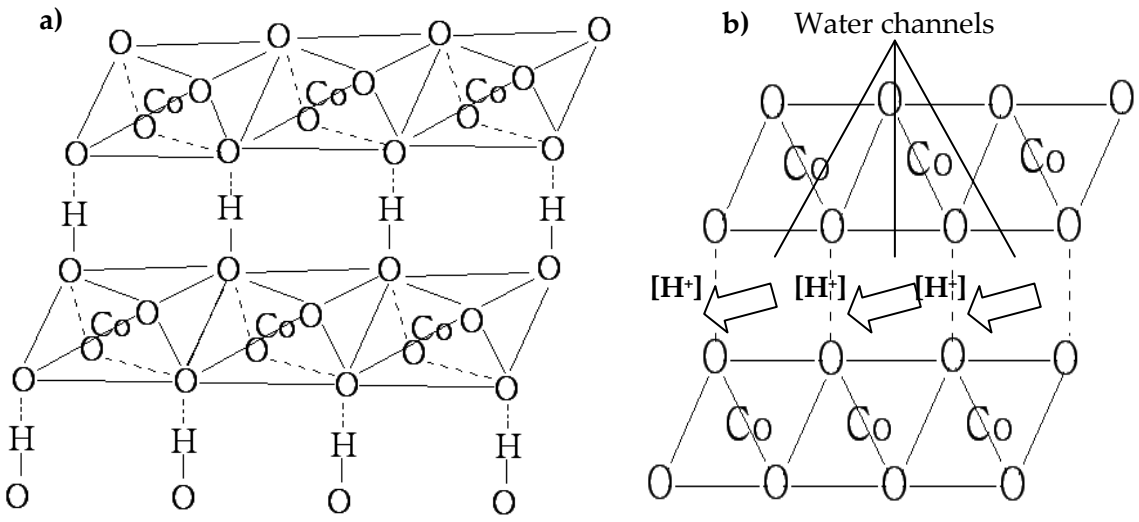

Figure 9: Spatial structure of CoOOH crystal (a) and a projection view of the crystal (b) (The figure was drawn based on contents in [44]). Hydrogen bonds are shown in dashed lines between hydrogen atoms and oxygen atoms. Spaces between layers of octahedrons allow water molecules to form water channels and conduct protons.

To test the proton conductivities of membranes derived from cobalt oxyhydroxides, cobalt-based nanoparticles need to be prepared. Cobalt oxyhydroxide (CoOOH) powders were purchased from GFS Chemicals (Powell, OH) and the size of CoOOH particles was reduced to nano-scale via the same processing methods as lepidocrocite (reaction with acetic acid and sonication). All specific procedures were exactly the same as those applied to treat lepidocrocite.

3.1.4 Preparation of iron-PVA and cobalt-PVA composite membranes

Polyvinyl alcohol (PVA) was selected as the backbone material of the composite membrane in my study because PVA is highly resistant against acid, alkali and organic reagents and the production cost of PVA is relatively low. Moreover, PVA

has very good mechanical properties and it has been shown to be a good host for various nanoparticle fillers [45-50]. Figure 10 shows the chemical structure of PVA polymer and the synthesis processes of PVA polymer.

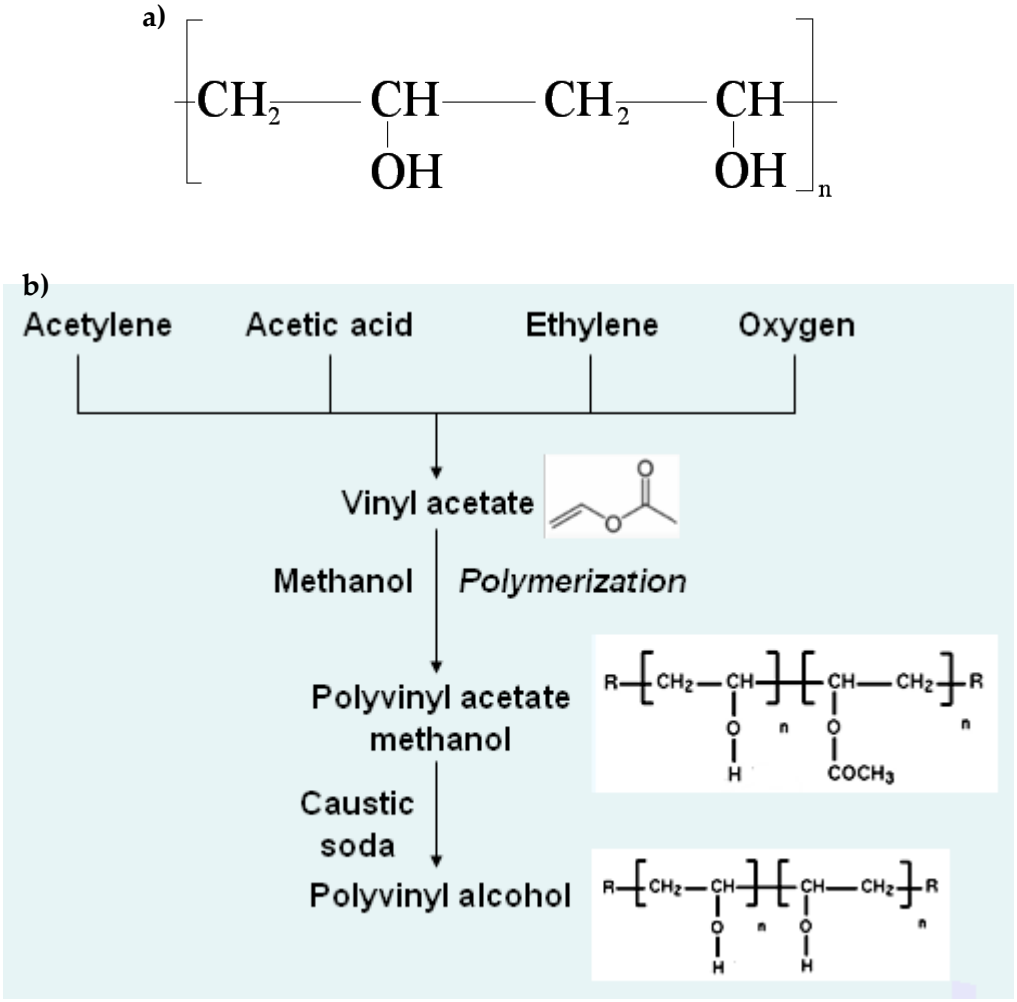

Figure 10: The chemical structure of PVA polymer (a) and the typical synthesis processes of PVA (b) (The figure was drawn based on the contents in [45])

The preparations of iron-PVA and cobalt-PVA composite membranes followed the same steps. A PVA solution was prepared via dissolving 3g of PVA powder (Fisher Scientific, Pittsburgh, PA) in 100 mL of the DDI water. The mixture was stirred over

night to make PVA powders completely dissolved in water. The solution was divided in several small beakers (20 mL each) and different amount of nanoparticles were added to every beaker to get samples with different PVA:nanoparticle mass ratios (PVA only, PVA:Ferroxane = 1:1.5, PVA:Ferroxane = 1:4, PVA: Lepidocrocite (sonication) = 1:4, PVA: carboxylate-CoOOH = 1:4 and PVA: CoOOH (sonication) = 1:4). All the mixtures were stirred at room temperature for 2 hours with the use of a magnetic stirrer plate (Corning Incorporated, Corning, NY) to make nanoparticles completely dissolved in the solutions. The solutions were air-dried in several Petri dishes at room temperature to get different iron-PVA and cobalt-PVA composite membrane samples.

3.1.5 Preparation of iron-polysulfone and cobalt-polysulfone composite membranes

Polysulfone was also tested as the backbone material in my study because previous studies have proven the reliance of polysulfone as a polymer material to synthesize proton-conductive composite membranes [40, 41]. Figure 11 shows the chemical structure of polysulfone. The synthesis of polysulfone is fairly complicated, which involves the nucleophilic substitution of 4,4'-dichlorodiphenyl sulfone with 4,4'-(1-methylethylidene)bisphenol in a aprotic solvent with high polarity but lacks hydrogen atoms connecting with oxygen atoms [51].

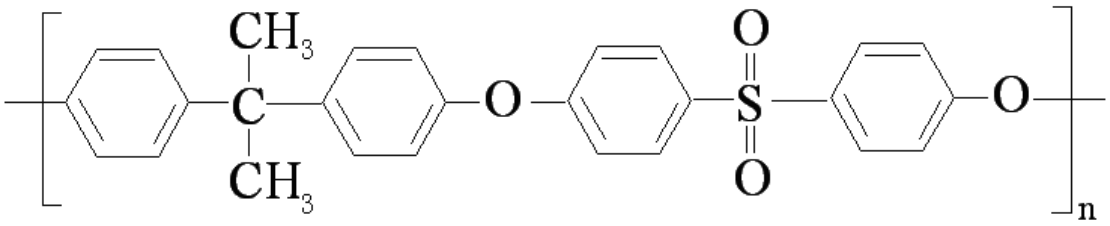

Figure 11: Chemical structure of Polysulfone

To produce iron-polysulfone and cobalt-polysulfone composite membranes, 1.2 g of lepidocrocite nanoparticles and CoOOH nanoparticles (prepared via sonication) were mixed with 43.7 mL of Dimethylformamide (DMF) (EMD Chemicals, Gibbstown, NJ), respectively. The mixtures were put in a sonication bath (Cole-Parmer Instrument Company, Vernon Hills, IL) and got sonicated for 10 minutes, so as to assure that the nanoparticles were homogeneously distributed in the DMF solvent. 8.5 g of solid polysulfone (Sigma-Aldrich Inc., St. Louis, MO) was then put into the DMF solvent and the whole mixture (polysulfone + DMF + nanoparticles) was stirred at room temperature for 24 hours with the use of a magnetic stirrer plate (Corning Incorporated, Corning, NY) so as to enable polysulfone to completely dissolve in DMF solvent. Two approaches were applied to get iron-polysulfone and cobalt-polysulfone composite membranes. One approach was to air-dry the mixtures and make the DMF solvent completely evaporated. This approach yielded a thick and rigid polysulfone membrane. The other approach was to cast the mixtures onto glass plates (form very thin layers on glass plates) and then immerse the glass plates into DDI water. The DMF solvent dissolved in water and a thin, soft polysulfone membrane was formed.

Proton conductivities of both membranes prepared via different methods were measured.

3.2 Membrane characterization methods

3.2.1 Electrochemical impedance spectroscopy (EIS)

Proton conductivity is the most important index that can evaluate the performance of a proton exchange membrane in the PEMFC system. Electrochemical Impedance Spectroscopy (EIS) is a widely used measurement method to determine the proton conductivity of PEMs. In the EIS measurement, a Nyquist plot (the real component of the system impedance vs. the negative of the imaginary component of the system impedance at various current frequencies) can be obtained [52]. Based on the plot and the corresponding equivalent circuit, the resistance of the PEM, R_s, can be obtained. The equivalent circuit for a typical PEM resistance measurement system and the ideal Nyquist plot for this system are shown in figure 12 and figure 13, respectively. In the Nyquist plot, the resistance of the PEM, R_s, is simply the value at the point where the Nyquist plot intersects with x coordinate. The proton conductivity of the membrane, σ , can be calculated with the value of R_s [18]:

$$\sigma = \frac{l}{R_s A}$$

Where l is the thickness of the membrane (cm), R_s is the resistance of the membrane (ohm) and A is the cross-sectional area of the membrane (cm^2).

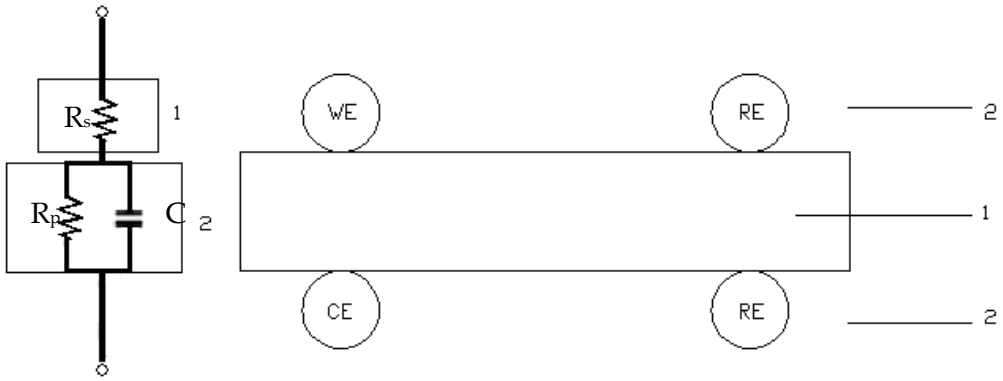

Figure 12: The equivalent circuit of the membrane impedance measurement system (drawn based on the contents in [53]). (1): Proton-conductive membrane sample. The resistance of the sample corresponds to R_s. (2): electrodes connected with potentiostat (WE, working electrode; CE, counter electrode; RE, reference electrode). The resistance of the interface between the sample and the electrodes and the capacitance between electrodes correspond to R_p and C, respectively [53].

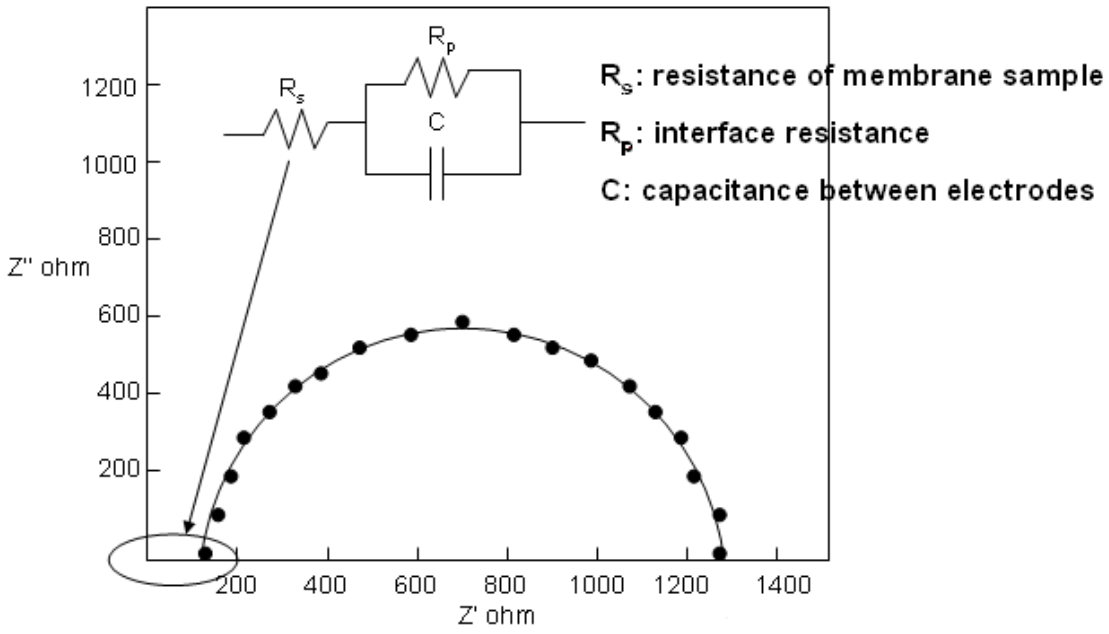

Figure 13: Nyquist plot corresponding to the equivalent circuit of the impedance measurement system. The resistance of the membrane sample (R_s) is obtained at the

intersection between the semi-circle Nyquist plot and x coordinate. (The figure is modified from [54])

In this work, the EIS measurements were conducted using a Gamry Potentiostat (Gamry Instruments, Inc., Warminster, PA) with program EIS 300 in Gamry Framework software system. Membrane sample was clamped by two plastic cylinders covered with aluminum foils and gold was sputtered on both sides of the sample with the use of a sputter coater. Copper wires were attached to aluminum foils and connected with the electrodes of the potentiostat. The schematic diagram of the measurement system is represented in figure 14.

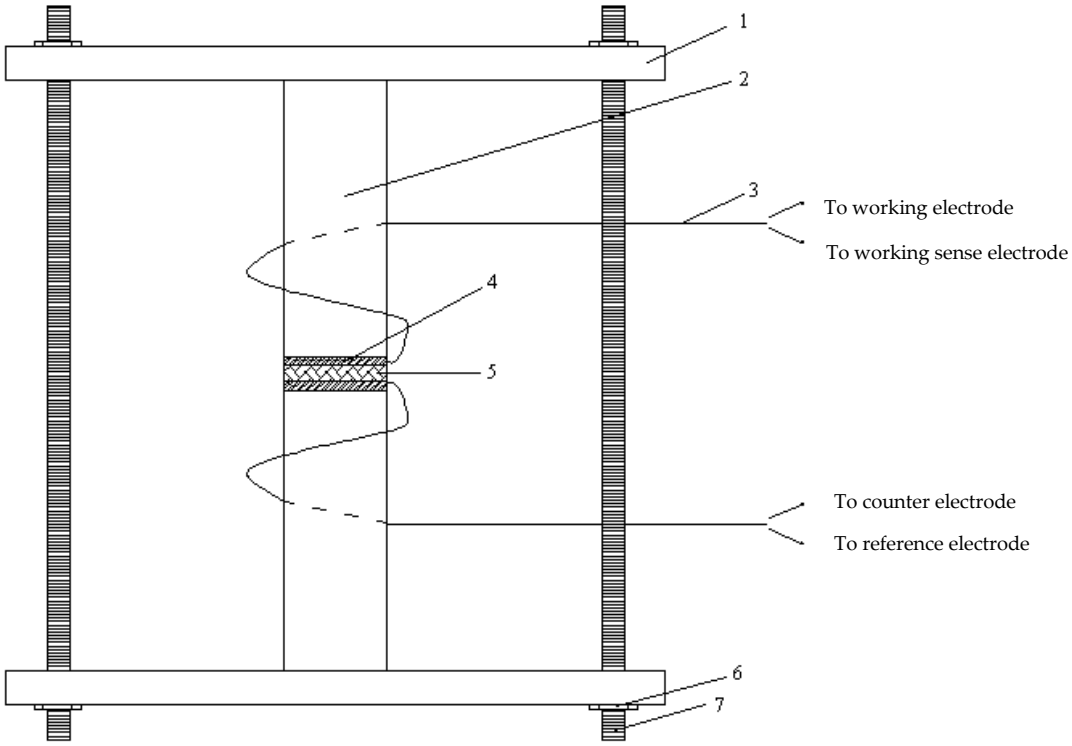

Figure 14

Figure 14: The schematic diagram of the membrane impedance measurement system. (1) plastic plate; (2) plastic cylinder; (3) copper wire; (4) aluminum foil; (5) membrane sample; (6) steel nut; (7) steel screw.

To create environments with different relative humidity values, various saturated salt solutions were put in sealed plastic cells and stood for 12h. Membrane samples were put in the cells and got equilibrated with the headspaces over the solutions in cells. The saturated salt solutions are $MgCl_2{\cdot}6H_2O$ for 33%RH, NaBr for 58% RH, $(NH_4)_2SO_4$ for 81% RH, K_2SO_4 for 97% RH and Millipore water 100% RH [18]. All experiments were conducted at room temperature (298K).

3.2.2 Attenuated total reflectance--Fourier transform infrared (ATR-FTIR) spectroscopy

Attenuated total reflectance-Fourier transform infrared (ATR-FTIR) spectroscopy is a unique surface sampling technique that obtains infrared spectra from the sample in contact with an optical sensor element [55]. It is a powerful tool to characterize the surface structure of the target substance. ATR-FTIR spectroscopy provides useful information of the functional groups on the surface of the sample, as well as information of any adsorption or desorption processes on sample surface and surface modification/etching of the sample, such as sputtering [56]. Advantages of the ATR-FTIR spectroscopy include the possibility to characterize sample surface and provide depth profiling of the sample without sectioning of the sample, feasibility to

deal with the sample with multi-phases and quick, easy obtaining of high-quality spectra [56, 57].

The principle of ATR-FTIR spectroscopy is shown in figure 15. An infrared beam is generated from an IR source and directed to the surface of the optical crystal. The beam will be reflected by the surface of the crystal and this internal reflectance can create an evanescent wave that passes through the surface of the crystal and gets into the sample held in contact with the crystal. If there is any functional group that possesses stretching vibrations between atoms, the energy of the evanescent wave will be absorbed by the vibrations and the evanescent wave will be attenuated. The signal of attenuated energy from each evanescent wave is passed back to the infrared beam, which then exits the crystal from the other side and the signal is passed to the detector in the IR spectrometer. The system then generates an infrared spectrum [58].

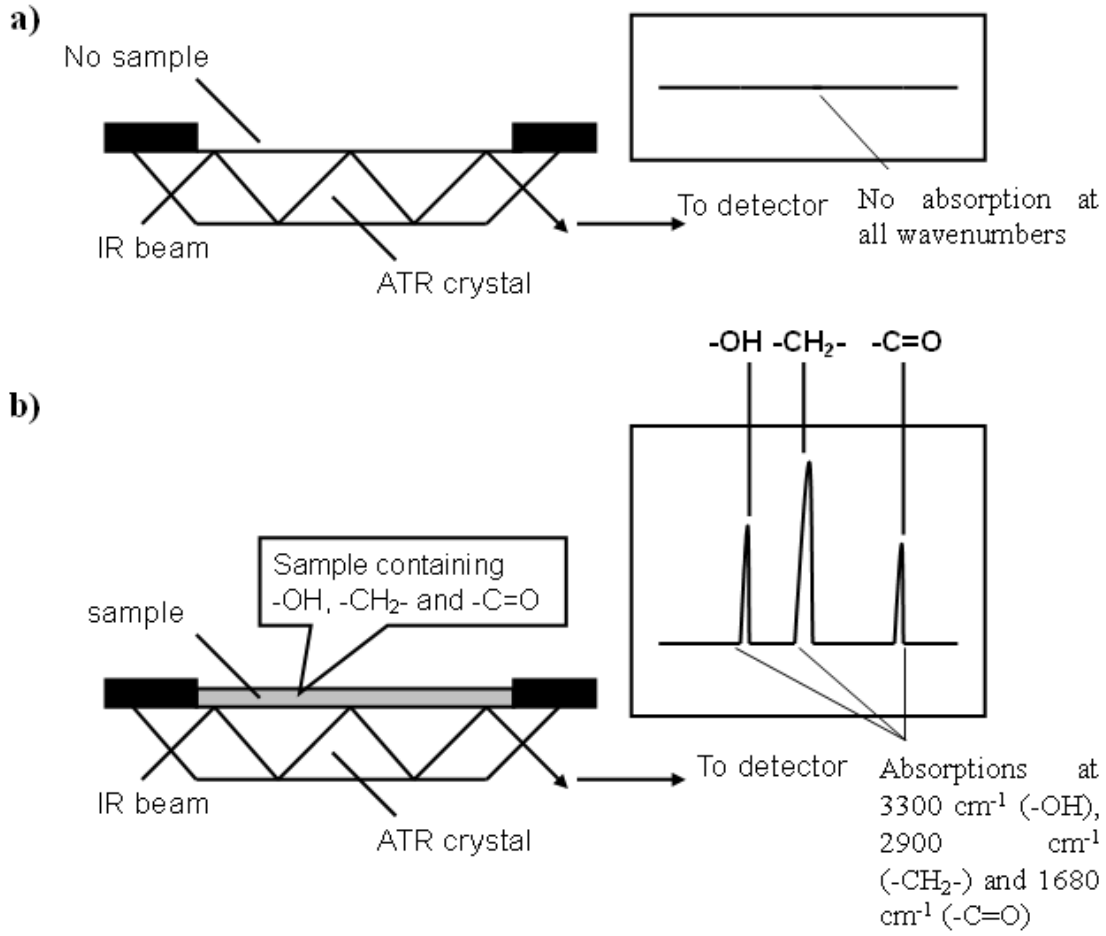

Figure 15: Principle of ATR-FTIR spectroscopy. When no sample is loaded (a), no attenuation of the evanescent wave occurs and the spectrum will be a straight line. When the sample containing functional groups is loaded (b), every functional group will selectively absorb energy from the evanescent wave with certain wavenumbers and the spectrum will show the absorption peaks of the evanescent wave at different wavenumbers.

ATR-FTIR spectra of the samples were obtained from a NexusTM 670 spectrometer (Nicolet Instrument Corporation, Madison, WI) with Smart Golden GateTM ATR bridge. The spectra were collected at wavenumbers ranged from 500 to

4000 cm^{-1} with an average of 64 scans. The software used to collect spectra is Omnic 5.1 software (Nicolet Instrument Corporation, Madison, WI).

3.2.3 Scanning electron microscope (SEM)

Scanning electron microscope (SEM) is a magnification instrument that applies high-energy electron beam to produce largely-magnified image. Since the 1st commercial SEM instrument was developed in 1965 by British Professor Charles Oatley, the SEM has experienced significant improvements and now the SEM has become one of the most powerful tools for the micro-scale exploration of composition, surface topography and crystal structure of samples. The advantages of SEM include: large depth of field (a large area of the sample can be in sharp focus simultaneously; as a result, the definition of the image produced by SEM is much better than that produced by a light microscope); high resolution, which allows the sample to be examined at a high magnification rate; wide range of magnification (usually between 10x and 100,000x), which meets the requirements of most users and are convenient for them to export images with appropriate magnification to computers [59].

The principle of SEM is displayed in figure 16. The electron beam is generated by the electron gun and the beam is accelerated by the attraction force produced by the anode. The beam is then condensed by the condense lens and focused by the objective lens as a tiny point on the surface of the sample. Once the beam of electrons hit the sample, an interaction between the beam and sample surface will occur and some free

electrons will be released as a result of the interaction (these electrons are referred as secondary electrons). At the same time, some electrons originally from the electron beam will be reflected and theses electrons are referred as primary backscattered electrons. Both primary backscattered electrons and secondary electrons are collected by individual detectors and are converted to electric signal (voltage). The level of the voltage signal controls the intensity of the magnetic field that deflects the spot of light projected on the surface of cathode-ray tube (CRT), so as to keep the intensity of the light spot on CRT surface the same as the intensity of electrons generated on the sample surface [59]. For example, if the electron beam hits the projection on the sample surface, a significant amount of primary backscattered electrons and secondary electrons will be generated and detected. These electrons contribute to a high level of voltage signal, thus results in a high intensity of the light spot on CRT surface (a bright spot). If the beam is then moved to a depressed site on the sample surface, fewer primary backscattered electrons and secondary electrons will be generated and that results in a low intensity of the light spot on CRT surface (a dark spot). The SEM image contains thousands of bright spots and dark spots on CRT surface, which corresponds to a profile of the topography of sample surface [59].

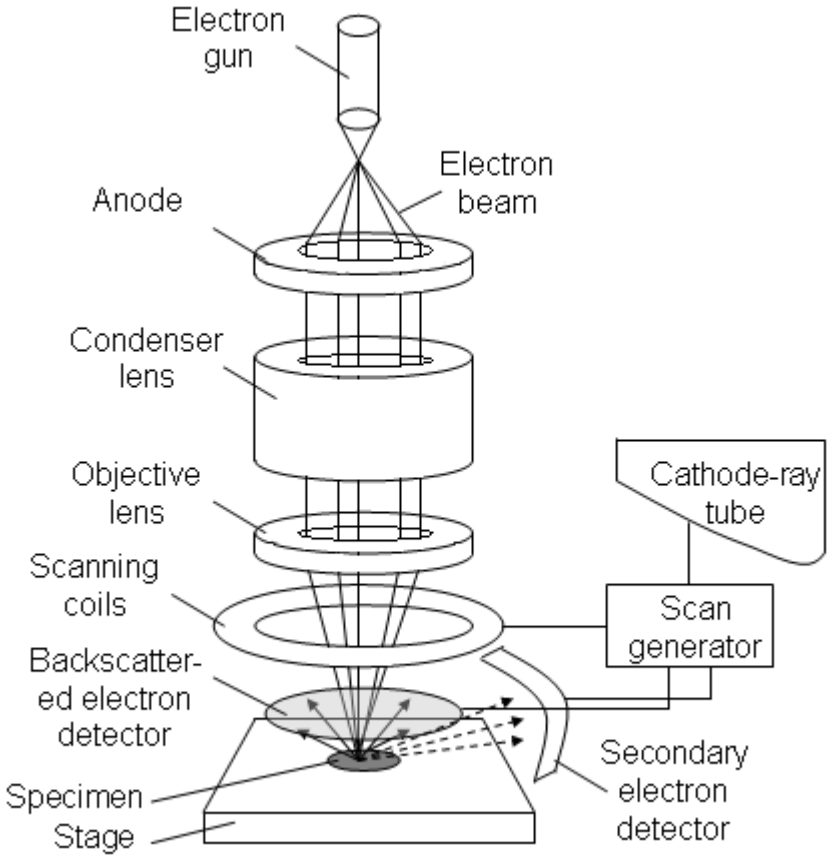

Figure 16: Schematic diagram of a SEM (The figure was redrawn based on the figures in [60])

To obtain SEM images with high qualities, special preparation of the sample is needed. Firstly, all water must be removed from sample surface, because the SEM utilizes a vacuum environment and water can evaporate in the vacuum and interfere with the electron beam. Secondly, the surface of sample needs to be conductive, so as to assure that the primary backscattered electrons and secondary electrons generated are beyond the detectable level. A thin layer of conductive material (gold or platinum)

can be sputtered on the surfaces of non-conductive samples to make the surfaces conductive [60].

Ferroxane-PVA composite membrane samples were imaged with a SEM (FEI XL30 SEM-FEG, FEI, Hillsboro, OR) in my experiments. Samples were attached to a circular copper plate and were sputtered with platinum to form a thin platinum layer on the surfaces of samples, so as to provide a conductive surface for imaging.

3.2.4 Tensile resistance measurement

Possessing high mechanical strength is a very important criterion for membrane samples, because a sample with high mechanical strength is easier to be handled during the preparation and installation processes and tends to possess long durability during the operation period. Tensile resistance is a key index to evaluate the mechanical strength of membrane samples. The tensile resistance can be characterized by the stress-strain curve, which describes the relationship between the axial stress of the specimen (can be calculated via dividing the axial load (N) by the cross-sectional area (m^2, A=width of the membrane (m) $\times$ thickness of the membrane (m)) and the axial strain (can be found by dividing the elongation length of the specimen by the initial length of the specimen [61]. The specimen will break apart when the stress load on the specimen reaches a certain high value, and the corresponding axial stress and axial strain are referred as ultimate stress and ultimate strain, respectively. A material with desired mechanical properties for the application of proton exchange membrane

tends to have both high ultimate stress and strain. The stress-strain curve can be obtained with the use of a dynamic mechanical analyzer. In my experiments, membrane samples were shaped as dumbbell and the size of each sample was precisely determined. Samples were clamped at certain positions and both the tensile force and strain were recorded by a computer connected to the tensile tester (Tinius Olsen 1000, Tinius Olsen Inc, Horsham, PA) to obtain a stress-strain curve. The ultimate strength (σ_B) and ultimate strain (ε_B) were recorded when the sample got broken.

4. Results and discussion

4.1 Proton conductivity

4.1.1 Proton conductivities of iron oxyhydroxide and cobalt oxyhydroxide green bodies

The proton conductivities of iron oxyhydroxide and cobalt oxyhydroxide nanoparticles that are processed by different size-reducing methods are shown in figure 17--21. It can be seen that at almost all RHs, iron-based nanoparticles had higher proton conductivities than cobalt-based nanoparticles, no matter what size-reducing method is applied. As is widely known, the proton conductivity of a given metal oxyhydroxide material mainly depends on two indexes--the specific surface area of the material and the capacity to capture water molecules from external environment at unit surface area, which can be referred as hydrophilicity. Therefore, an in-depth investigation on the specific surface areas and hydrophilicities of FeOOH and CoOOH nanoparticles is made.

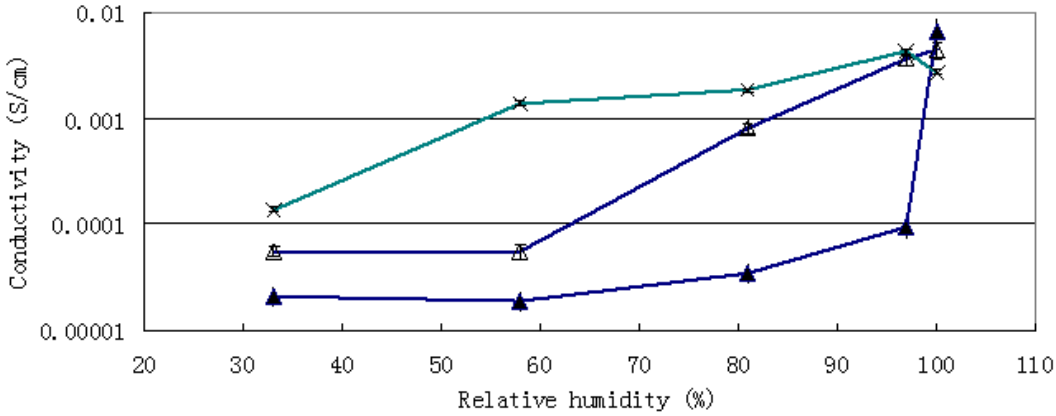

Figure 17

Figure 17: Comparison of proton conductivities of iron oxyhydroxide and cobalt oxyhydroxide nanoparticles prepared only by reaction with acetic acid. △= Lepidocrocite nanoparticles, the average thickness of the ceramic is 0.022 cm ± 2.2×10^{-3} cm; ▲= Cobalt nanoparticles, the average thickness of the ceramic is 0.022 cm ± 4.7×10^{-3} cm; ×= Nafion, the average thickness of Nafion is 0.013 cm ± 6.4×10^{-4} cm and the Nafion membranes used in the experiments were purchased from Ion Power, Inc (New Castle, DE).

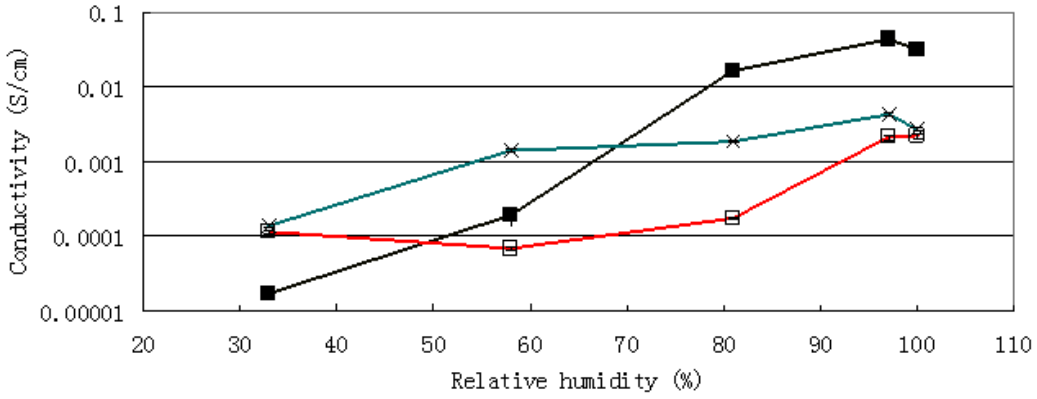

Figure 18: Comparison of proton conductivities of iron oxyhydroxide and cobalt oxyhydroxide nanoparticles prepared by sonication. ■= Lepidocrocite nanoparticles, the average thickness of the ceramic is 0.021 cm ± 2.5×10^{-3} cm; □= Cobalt oxyhydroxide nanoparticles, the average thickness of the ceramic is 0.025 cm ± 1.2×10^{-3} cm; ×= Nafion, the average thickness of Nafion is 0.013 cm ± 6.4×10^{-4} cm.

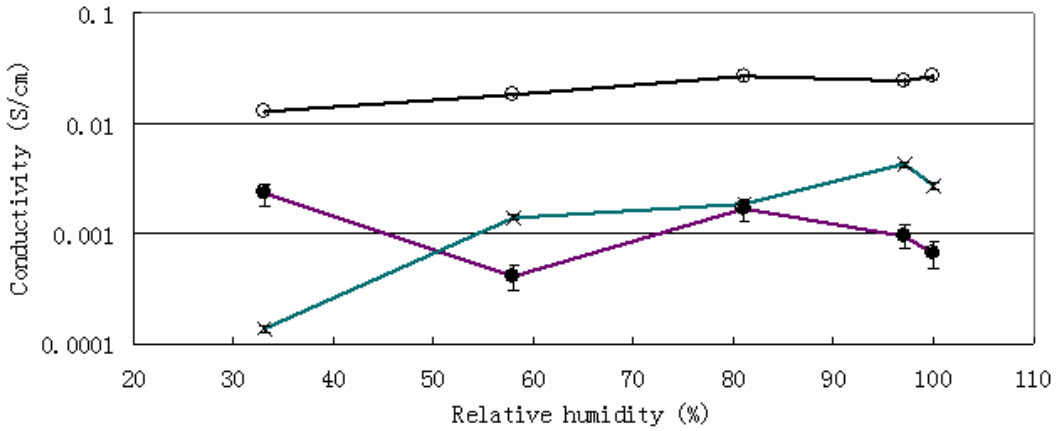

Figure 19: Comparison of proton conductivities of iron oxyhydroxide and cobalt oxyhydroxide nanoparticles prepared by reaction with acetic acid + sintering at 300 ℃. ○= Lepidocrocite nanoparticles, the average thickness of the ceramic is 0.030 cm ± 1.4×10^{-3} cm; ●= Cobalt oxyhydroxide nanoparticles, the average thickness of the ceramic is 0.031 cm ± 7.2×10^{-3} cm; ×= Nafion, the average thickness of Nafion is 0.013 cm ± 6.4×10^{-4} cm.

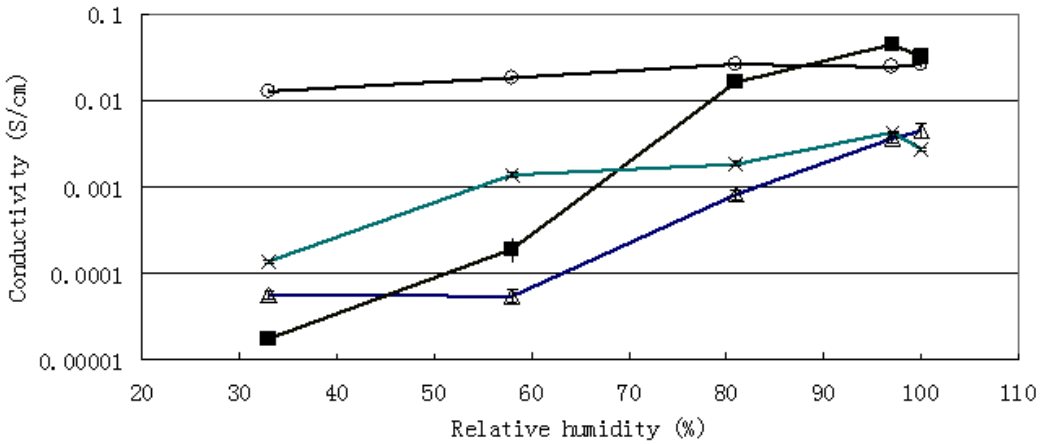

Figure 20: Comparison of proton conductivities of iron oxyhydroxide nanoparticles prepared by different size-reducing method. ○= Lepidocrocite reacted with acetic acid and then sintered at 300 ℃, the average thickness of the ceramic is 0.030 cm ± 1.4×10^{-3} cm; ■= Lepidocrocite treated by sonication, the average thickness of the ceramic is 0.021 cm ± 2.5×10^{-3} cm; △= Lepidocrocite reacted with acetic acid, the

average thickness of the ceramic is 0.022 cm ± 2.2×10^{-3} cm; ×= Nafion, the average thickness of Nafion is 0.013 cm ± 6.4×10^{-4} cm.

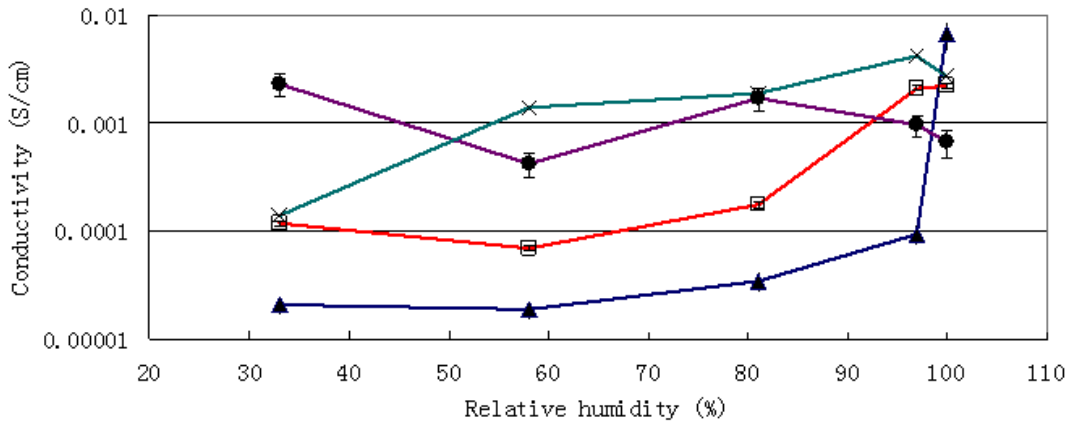

Figure 21: Comparison of proton conductivities of cobalt oxyhydroxide nanoparticles prepared by different size-reducing method. ●= Cobalt oxyhydroxide reacted with acetic acid and then sintered at 300 ℃, the average thickness of the ceramic is 0.031 cm ± 7.2×10^{-3} cm; □= Cobalt oxyhydroxide treated by sonication, the average thickness of the ceramic is 0.025 cm ± 1.2×10^{-3} cm; ▲= Cobalt nanoparticles, the average thickness of the ceramic is 0.022 cm ± 4.7×10^{-3} cm; ×= Nafion, the average thickness of Nafion is 0.013 cm ± 6.4×10^{-4} cm.

Both CoOOH and FeOOH material possess very large active surface areas [62]. The specific surface area of CoOOH nanoflake film is around 100.0 m^2/g [63], while the specific surface area of FeOOH nanoparticles is around 96.0 m^2/g [18]. Though the specific surface area of CoOOH nanoparticles used in my experiments may be lower than that of CoOOH nanoflake films reported in [63], the surface areas of CoOOH and FeOOH are still expected to be in the same range. Therefore, the significant gap between the proton conductivities of CoOOH and FeOOH can not be explained in the aspect of specific surface area.

The hydrophilicity data of CoOOH can not be found through article search. However, based on the results from a previous study, we can infer that the hydrophilicity of CoOOH is lower than that of FeOOH. Casey and Westrich published their results on mineral dissolution rates in Nature in 1992, which revealed that orthosilicate minerals containing cobalt tended to have a lower dissolution rate than orthosilicate minerals containing iron. This result was explained by the lower water exchange rate from the bulk into the hydration sphere of cobalt, compared with iron [64]. Though the crystal structure of CoOOH is quite different from that of cobalt-based orthosilicate, the fact that cobalt atoms have a lower tendency to attract water molecules than that of iron atoms is solid. Therefore, compared with FeOOH, less water molecules can be adsorbed on CoOOH surface at the given RH and the rate of proton exchange on CoOOH surface is restricted. As a result, the proton conductivity of CoOOH tends to be lower than FeOOH.

Both FeOOH and CoOOH treated via sonication tended to have proton conductivities higher than corresponding FeOOH and CoOOH treated only by the reaction with acetic acid. That can be interpreted as the effect of introduced acetic acid groups on surfaces of acetic acid--treated samples. As discussed in previous section, the existence of acetic acid groups can hinder the transfer of protons and reduces the proton conductivity of samples. When the acetic acid--treated samples were heated at 300℃ for 4 hours, the proton conductivities of these samples became much higher.

Therefore, we can draw the conclusion that sintering at high temperature is an effective way to remove acetic acid groups on the surfaces of FeOOH and CoOOH particles and nanoparticles obtained from the treatment of acetic acid + sintering are suitable for the applications at low and moderate RHs. In contrast, nanoparticles obtained from the treatment of sonication are suitable for the applications at high RHs.

4.1.2 Impact of PVA:Fe ratio on the proton conductivity of ferroxane-PVA composite membrane

Figure 22 shows the proton conductivities of various membrane samples. It is clear that the ferroxane--PVA composite membranes had higher proton conductivity than the pure PVA membrane, and the membrane with high ferroxane content (PVA:Fe = 1:4, mass ratio) displayed a higher proton conductivity than the membrane with low ferroxane content (PVA:Fe = 1:1.5, mass ratio), because of the strong water adsorption capacity of the ferroxane nanoparticles. The composite membrane with PVA:Fe =1:4 (mass ratio) had proton conductivities comparable with those of the Nafion membrane at RHs above 81%, which illustrates a potential for the composite membrane to be applied in PEMFCs at high RHs. However, the proton conductivity of the composite membrane dropped very significantly at low RHs, which is due to two reasons: the loss of hydroxyl groups from ferroxane surfaces during the combination of ferroxane nanoparticles and PVA and the existence of acetic acid groups connected with Fe atoms in ferroxane nanoparticles. Though acetic acid groups can be removed during the sintering process (300℃ for 4-5 hours) and the hindering effect can be

extinguished [18], the composite membrane can not be treated in that way, because the membrane can not endure high sintering temperature (the melting point of PVA is 228 ℃ [65]) and will get burned if the sintering temperature reaches 300 ℃.

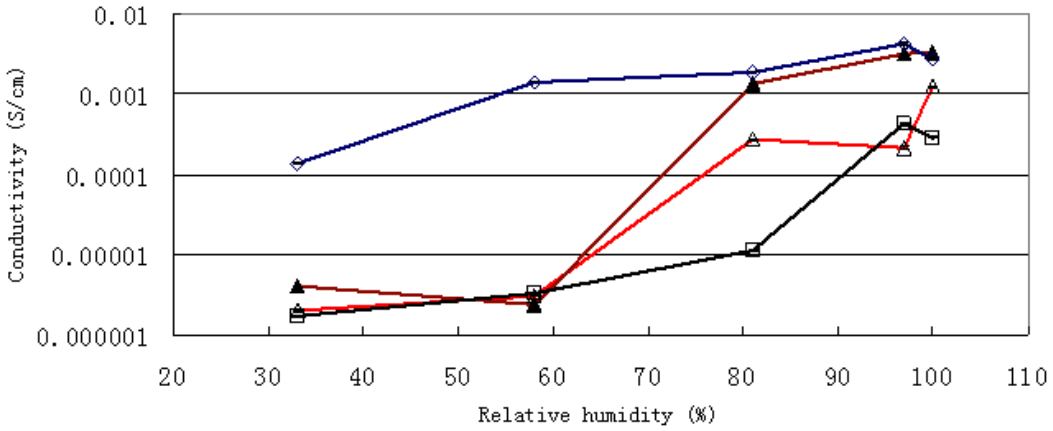

Figure 22: Proton conductivities of Nafion (◇, average thickness= 0.013 cm ± 6.4×10^{-4} cm), pure PVA (□, average thickness= 0.020 cm ± 7.8×10^{-4} cm) and ferroxane-PVA composite membranes with different PVA:Fe ratios (PVA:Fe=1:1.5 (△, average thickness= 0.025 cm ± 1.2×10^{-3} cm) and PVA:Fe=1:4 (▲, average thickness= 0.025 cm ± 1.1×10^{-3} cm), mass ratio) at various relative humidities.

4.1.3 Comparison of proton conductivities of Fe-PVA and Co-PVA composite membranes

Figure 23 shows the proton conductivities of various Fe-PVA and Co-PVA composite membranes. It can be seen that the proton conductivities of Fe-PVA membranes were much higher than those of Co-PVA composite membranes, which corresponds well with the results of iron oxyhydroxide and cobalt oxyhydroxide nanoparticles. In particular, the proton conductivity of lepidocrocite-PVA composite membrane (lepidocrocite fillers were reduced to nano-scale via sonication) was extremely high at high relative humidities (0.00654 S/cm at 81% and 0.0106 S/cm at

97%), which was 2-3 times higher than that of Nafion (0.00187 S/cm at 81% and 0.00426 S/cm at 97%). All membrane samples with metal oxyhydroxide fillers treated via sonication had proton conductivities higher than the corresponding samples with fillers treated only via the reaction with acetic acid, which proves that the use of acetic acid can introduce unwanted acetic acid groups to the surface of metal oxyhydroxide fillers and these groups deteriorate the proton conductivities of composite membranes. Similar to the results in section 4.1.2, all of the composite membranes tested had extremely low proton conductivities at low RHs (Maximum proton conductivities were 4.73×10^{-6} S/cm at 33% RH and 5.18×10^{-6} S/cm at 58% RH, while the proton conductivities of Nafion were 1.38×10^{-4} S/cm at 33% RH and 1.4×10^{-3} S/cm at 58% RH). Considering the fact that all of the FeOOH and CoOOH nanoparticles tested had proton conductivities above 10^{-5} S/cm at low RHs, we can draw the conclusion that the introduction of PVA to the metal oxyhydroxide nanoparticles inevitably decreases the proton conductivities of metal oxyhydroxide nanoparticles and during the mixing process of PVA and metal oxyhydroxide nanoparticles, certain amount of hydroxyl groups on the surfaces of metal oxyhydroxide nanoparticles may get substituted or encapsulated by PVA polymer.

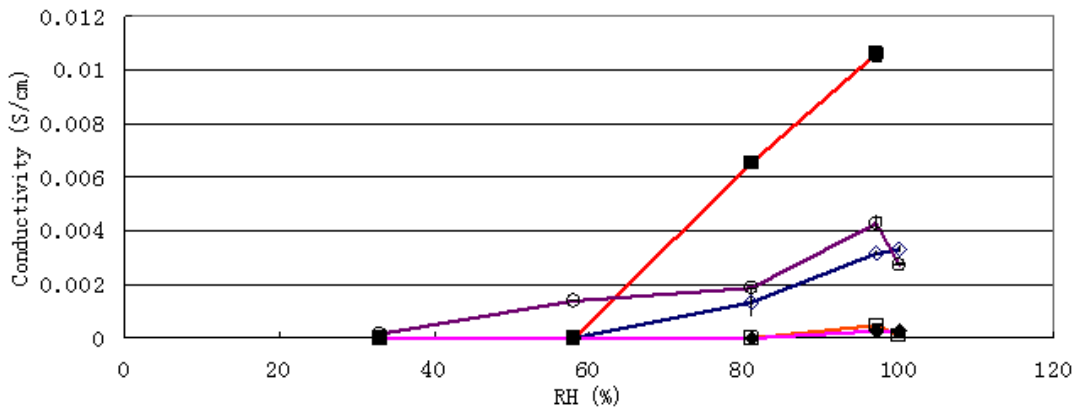

Figure 23: Proton conductivities of Fe-PVA and Co-PVA composite membranes. All composite membrane samples have the same PVA : metal oxyhydroxide mass ratio (1:4). ■= Lepidocrocite nanoparticles prepared by sonication + PVA, average membrane thickness= 0.060 cm ± 4.80×10^{-3} cm; □= Cobalt oxyhydroxide nanoparticles prepared by sonication + PVA, average membrane thickness= 0.032 cm ± 2.2×10^{-3} cm; ◇= Lepidocrocite nanoparticles prepared by reaction with acetic acid + PVA, average membrane thickness= 0.025 cm ± 1.1×10^{-3} cm; ◆= Cobalt oxyhydroxide nanoparticles prepared by reaction with acetic acid + PVA, average membrane thickness= 0.030 cm ± 4.0×10^{-3} cm; ○= Nafion, average thickness= 0.013 cm ± 6.4×10^{-4} cm. The composite membranes with FeOOH and CoOOH particles prepared by reaction with acetic acid + calcination were not tested, because the FeOOH and CoOOH nanoparticles prepared by reaction with acetic acid + calcination did not dissolve in the PVA solution during the synthesis process of the composite membranes. Therefore, it is impossible to produce the composite membranes with FeOOH and CoOOH nanoparticles homogeneously distributed in the membranes.

4.1.4 Comparison of proton conductivities of Fe-Polysulfone and Co-Polysulfone composite membranes

Figure 24 shows the proton conductivities of Fe-polysulfone and Co-polysulfone composite membranes. Compared with PVA-based composite membranes, the proton conductivities of polysulfone-based composite membranes were quite low (conductivities of most samples were in the range of 10^{-6}--10^{-5} S/cm. Even at high RHs

(above 81%), the highest conductivity value was only 1.84×10^{-5} S/cm (FeOOH + polysulfone, treated by evaporation method at 100% RH), which was only one thousandth of the conductivity value of the corresponding FeOOH + PVA membrane (0.0106 S/cm at 97%RH). Therefore, Polysulfone is not a good candidate for the polymeric backbone of the metal oxyhydroxide-based composite membrane. Most FeOOH-based samples had proton conductivities higher than corresponding CoOOH-based samples, which was consistent with the results of FeOOH and CoOOH nanoparticles. Samples prepared via evaporation method had proton conductivities higher than samples prepared via casting method, because casting method involves the immersion of samples into water and some FeOOH and CoOOH nanoparticles may dissolve in water during the immersion process.

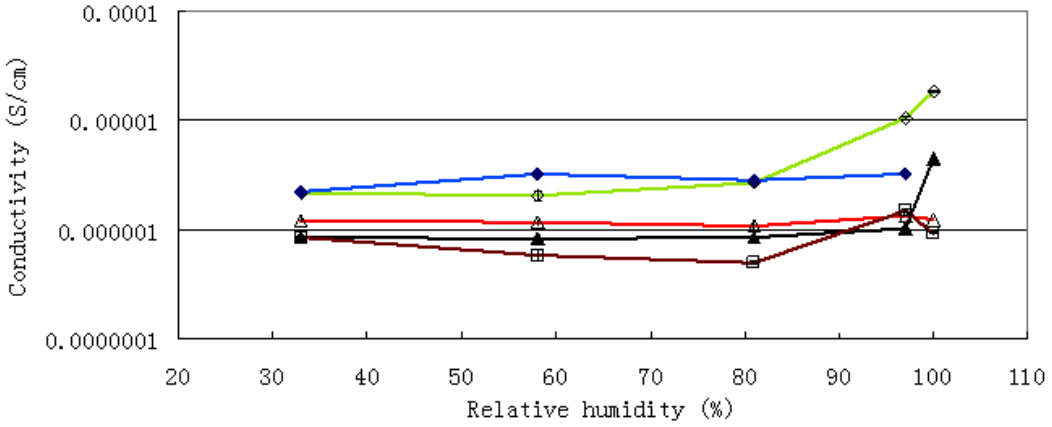

Figure 24: Proton conductivities of FeOOH-polysulfone and CoOOH-polysulfone composite membranes. △= FeOOH nanoparticle + polysulfone (prepared by casting method, average membrane thickness =0.013 cm ± 2.2×10^{-3} cm); ▲= CoOOH nanoparticle + polysulfone (prepared by casting method, average membrane thickness =0.012 cm ± 3.5×10^{-3} cm); ◇= FeOOH nanoparticle + polysulfone

(prepared by solvent evaporation method, average membrane thickness =0.019 cm ± 7.7×10^{-4} cm); ◆= CoOOH nanoparticle + polysulfone (prepared by solvent evaporation method, average membrane thickness =0.045 cm ± 7.5×10^{-3} cm); □= Polysulfone only, average membrane thickness =0.0076 cm ± 6.5×10^{-4} cm.

4.2 ATR-FTIR

4.2.1 ATR-FTIR images of FeOOH and CoOOH green bodies

Figure 25 shows the ATR-FTIR spectra of FeOOH, CoOOH, FeOOH (reacted with acetic acid) and CoOOH (reacted with acetic acid). Generally speaking, the ATR-FTIR curves of FeOOH and CoOOH were very similar, due to the similarity of covalence bonds in FeOOH and CoOOH crystals. Moderate absorption peaks at around 3350 cm^{-1} were observed in both samples (①), which represent the existence of O-H vibration. Both FeOOH and CoOOH samples had strong absorption at around 2900 cm^{-1} (②) and that can be interpreted as the existence of special O-H bonds that are in interaction with other nearby atoms [66]. The absorption peak of lepidocrocite at around 2900 cm^{-1} was much more significant than other absorption peaks, while the absorption peak of cobalt oxyhydroxide at 2900 cm^{-1} was not that significant. Therefore, the surface density of -OH groups of lepidocrocite might be higher than that of cobalt oxyhydroxide and that can contribute to a higher proton conductivity of lepidocrocite, which is consistent with the proton conductivity results in section 4.1.1.. Both FeOOH and CoOOH samples had absorption at around 1610 cm^{-1} (③), which can be interpreted as the existence of Fe-O double bonds in the crystal structures of FeOOH and CoOOH [66, 67].

The ATR-FTIR image of FeOOH reacted with acetic acid showed slight differences from the ATR-FTIR image of raw FeOOH. Firstly, the relative absorption intensity at around 2900 cm^{-1} (②) decreased when raw FeOOH reacted with acetic acid, because the reaction with acetic acid can result in the reduction of -OH groups (some -OH groups are substituted with CH_3COO- groups). Secondly, the relative absorption intensity at around 1610 cm^{-1} (③) increased, partly due to the introduction of C=O double bonds from acetic acid to the surface of FeOOH. The ATR-FTIR image of CoOOH reacted with acetic acid did not illustrate significant differences from that of raw CoOOH.

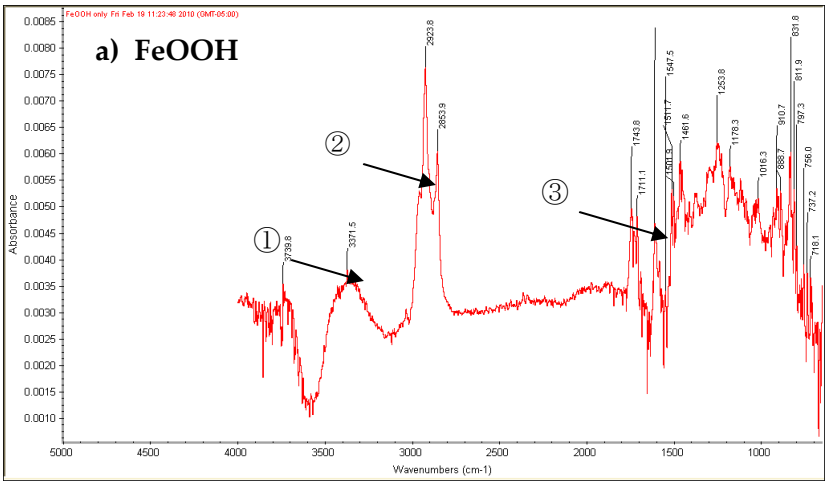

Figure 25

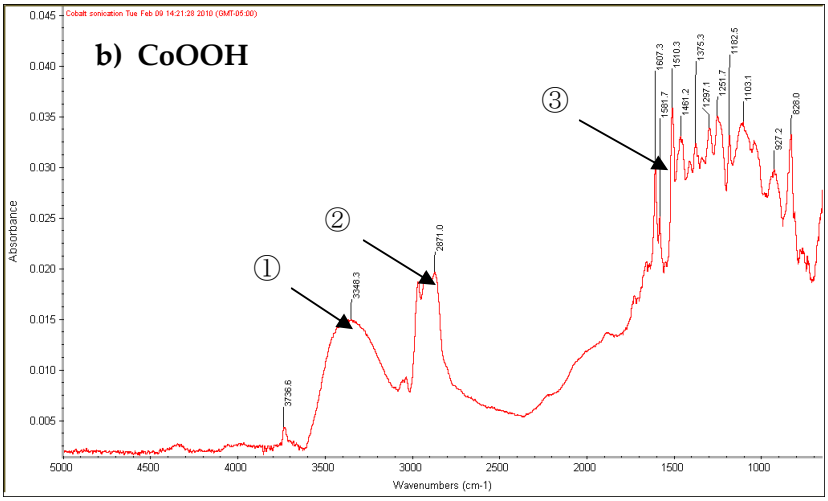
b) CoOOH
Absorbance
Wavenumbers (cm-1)
①
②
③
3736.6
3346.3
2871.0
1607.3
1581.7
1510.3
1461.2
1375.3
1297.1
1251.7
1182.5
1103.1
927.2
828.0

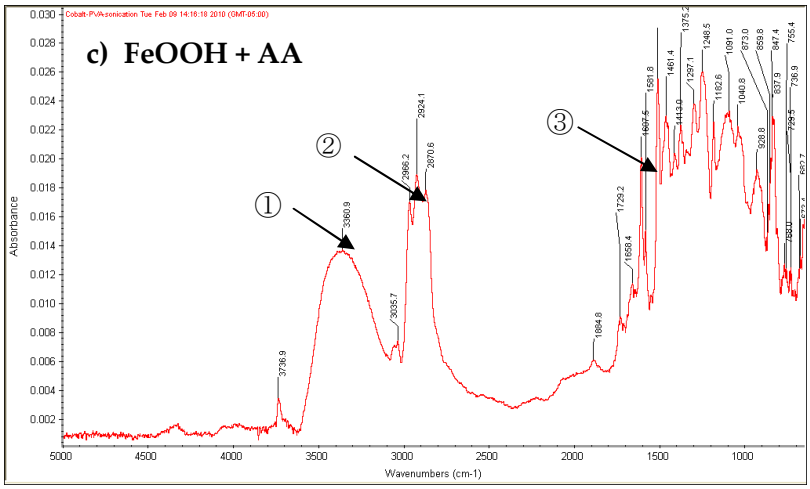
c) FeOOH + AA
Absorbance
Wavenumbers (cm-1)
①
②
③
3736.9
3360.9
3035.7
2966.2
2924.1
2870.6
1894.8
1729.2
1668.4
1581.8
1461.4
1375.2
1297.1
1248.5
1182.6
1091.0
1040.8
928.8
637.9
847.4
755.4
736.9

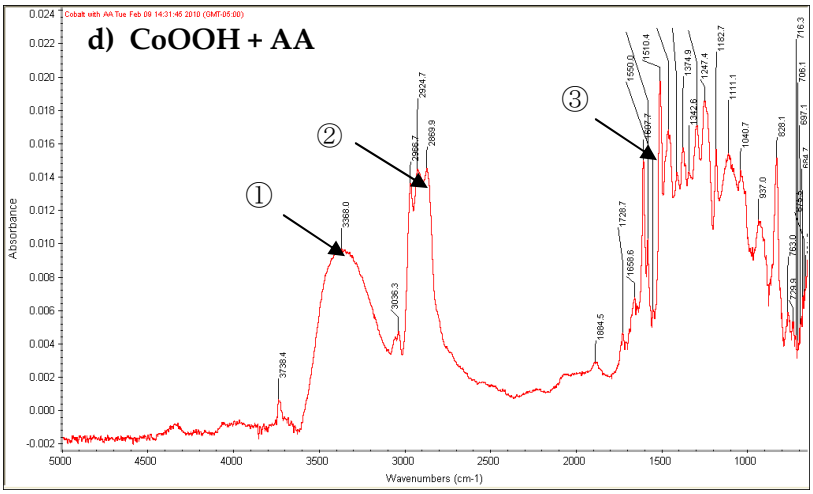
d) CoOOH + AA
Absorbance
Wavenumbers (cm-1)
①
②
③
3738.4
3368.0
3036.3
2966.7
2924.7
2869.9
1894.5
1728.7
1658.6
1550.0
1510.4
1374.9
1247.4
1182.7
1111.1
1040.7
937.0
828.1
716.3
706.1
697.1
694.7

Figure 25

Figure 25: ATR-FTIR spectra of a) FeOOH nanoparticles prepared via sonication; b) CoOOH nanoparticles prepared via sonication; c) FeOOH nanoparticles prepared via the reaction with acetic acid; d) CoOOH nanoparticles prepared via the reaction with acetic acid.

4.2.2 ATR-FTIR images of Fe-PVA and Co-PVA composite membranes

Figure 26 shows the ATR-FTIR images of pure PVA polymer, PVA filled with FeOOH nanoparticles (processed by sonication), PVA filled with CoOOH nanoparticles (processed by sonication), PVA filled with FeOOH nanoparticles (reacted with acetic acid) and PVA filled with CoOOH nanoparticles (reacted with acetic acid), respectively. Characteristic absorption peaks of pure PVA included 3,340.2 cm^{-1} (-OH stretching vibrations, ①), 2920.3 cm^{-1} (CH/CH_2 stretching vibrations, ②), 1730.8 cm^{-1} (C-O stretching vibrations, ③), 1256.4 cm^{-1} and 1092.1 cm^{-1} (bands related to CH/CH_2 deformation vibrations, ④ and band of CO stretching vibrations, ⑤) [68]. Compared with the spectrum of pure PVA, the spectrum of PVA filled with FeOOH nanoparticles (processed by sonication) showed a much stronger absorption band at around 2900 cm^{-1} (②), which is consistent with the spectrum of pure FeOOH. Considering that the ATR-FTIR spectra mainly represent the surface properties of the samples tested, this result reveals the fact that a large proportion of FeOOH nanoparticles are distributed on the surface of the composite membrane and this can contribute to high proton conductivity of the sample, as the FeOOH nanoparticles on the surface of the sample are easier to catch free water molecules from external environment. In contrast, the spectra of sample (c), sample (d) and sample (e) did not

show significant absorption increases at around 2900 cm^{-1}, which means that the surface properties of these samples do not differ much from that of pure PVA sample and this results in lower proton conductivities of these samples. Absorption bands at around 1610 cm^{-1} (⑥) were observed in the spectra of (b), (c) and (e), which can be interpreted as the existence of acetic C=O bonds, Fe-O double bonds and Co-O double bonds [66, 67]. The spectrum of (d) did not display any absorption at around 1610 cm^{-1}.

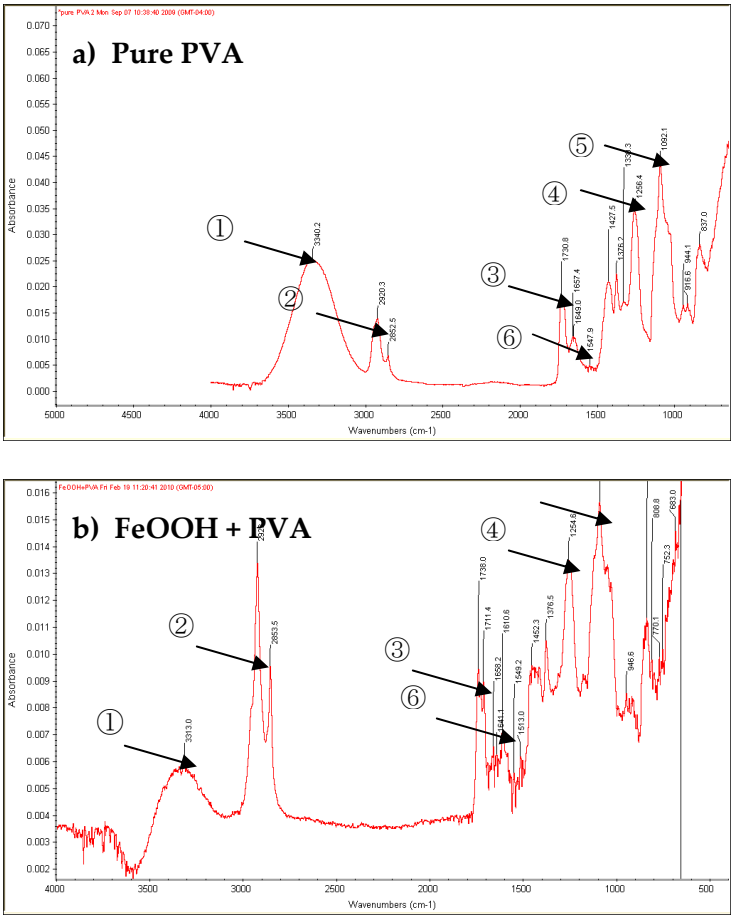

Figure 26

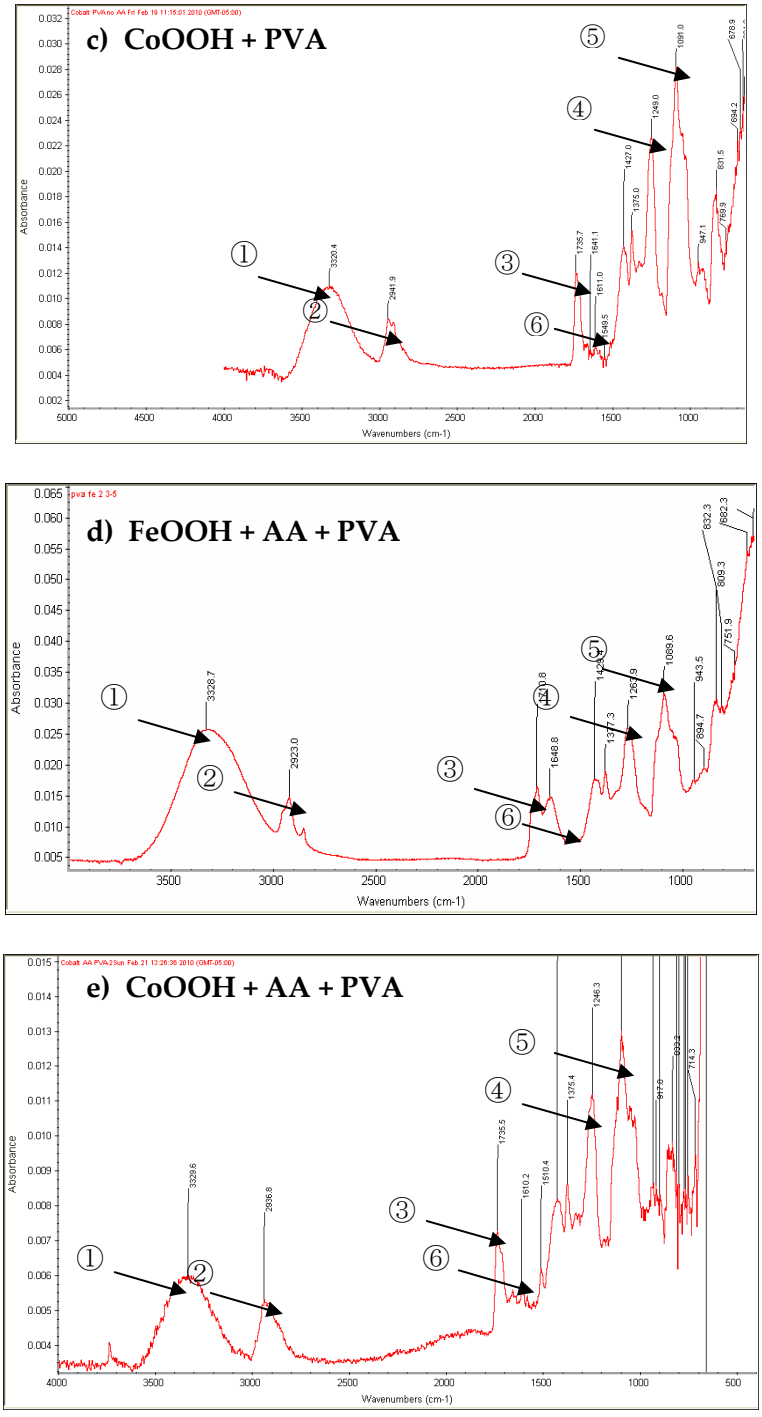

Figure 26: ATR-FTIR images of Fe-PVA and Co-PVA composite membranes. a): Pure PVA; b) FeOOH nanoparticles + PVA (nanoparticles obtained via sonication); c) CoOOH nanoparticles + PVA (nanoparticles obtained via sonication); d) FeOOH

nanoparticles + PVA (nanoparticles obtained via reaction with acetic acid); e) CoOOH nanoparticles + PVA (nanoparticles obtained via reaction with acetic acid).

4.2.3 ATR-FTIR images of Fe-Polysulfone and Co-Polysulfone composite membranes

Figure 27 shows the ATR-FTIR images of polysulfone polymer, polysulfone filled with lepidocrocite nanoparticles (processed via sonication) and polysulfone filled with cobalt oxyhydroxide nanoparticles (processed via sonication), respectively. When pure PSF was tested, a small absorption peak at 2969 cm^{-1} was observed, which refers to C-H stretching [69]. Other characteristic absorptions included absorption peaks at 1586 and 1488 cm^{-1} (aromatic bands) and 1411 cm^{-1} and 1364 cm^{-1} (methyl groups) [69].When polysulfone was filled with FeOOH and CoOOH nanoparticles, high absorptions at around 3300 cm^{-1} and 2900 cm^{-1} were expected, because both FeOOH and CoOOH nanoparticles have very strong absorptions at these two wavenumbers. However, the spectra of FeOOH + PSF polymer and CoOOH + PSF polymer were almost the same as that of pure PSF polymer and no significant absorption increases at 3300 cm^{-1} and 2900 cm^{-1} were observed. Considering that the ATR-FTIR spectra mainly represent the surface properties of the samples tested, we can make a conclusion that the FeOOH and CoOOH nanoparticles are “encapsulated” inside the skeleton of PSF and the distribution of these proton-conductive nanoparticles on the surfaces of the composite membranes is rare. As a result, the proton conductivities of polysulfone-based composite membranes are not high.

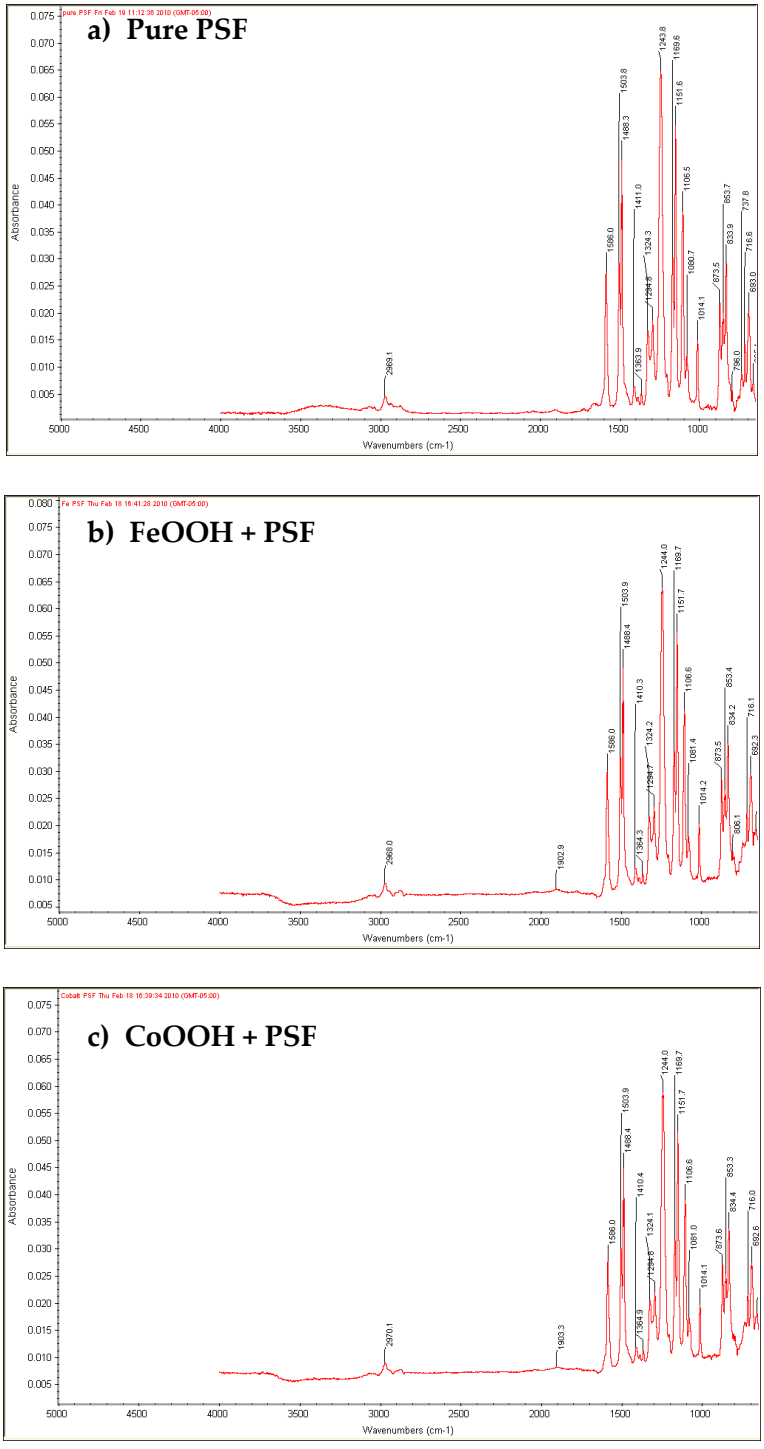

Figure 27: ATR-FTIR spectra of pure PSF polymer (a), lepidocrocite nanoparticles (prepared via sonication) + PSF (b) and cobalt oxyhydroxide nanoparticles (prepared via sonication) + PSF (c). All composite membranes are prepared via casting method.

4.3 SEM

Figure 28 and 29 show the SEM images of the surface and the cross-section of the ferroxane + PVA composite membrane (PVA:Fe mass ratio=1:4), respectively. Both figures revealed that in the ferroxane-PVA composite membrane, PVA acted as the backbone and ferroxane particles were distributed both on the surface and in the internal structure of PVA backbone. These ferroxane particles performed as the channels for proton conduction through the membrane. However, it could be seen that the ferroxane particles were not homogeneously distributed among the membrane. Aggregations of ferroxane particles occurred at both the surface and the inner space of the composite membrane (figure 29) and the average size of isolated ferroxane particles (~1000 nm) shown in figure 28 was much higher than the average diameter of ferroxane nanoparticles used in the PVA-ferroxane mixing process (D=60.2 ± 1.2 nm, measured by dynamic light scattering (DLS) using an ALV/CGS-3 Compact Goniometer System (ALV-GmbH, Germany)). This result can be used to explain why the ferroxane-PVA composite membrane tends to have lower proton conductivity than that of the ferroxane nanoparticles, especially at low RHs. To be specific, the aggregation of ferroxane nanoparticles (the aggregation may occur at either mixing process or water-evaporation process) decreases the specific surface area of ferroxane in the composite membrane and that will result in a decrease of proton conductivity. Therefore, the development of approaches to avoid the aggregation of ferroxane

nanoparticles during the preparation process of composite membranes is needed for the improvement of proton-conducting performance of the composite membrane.

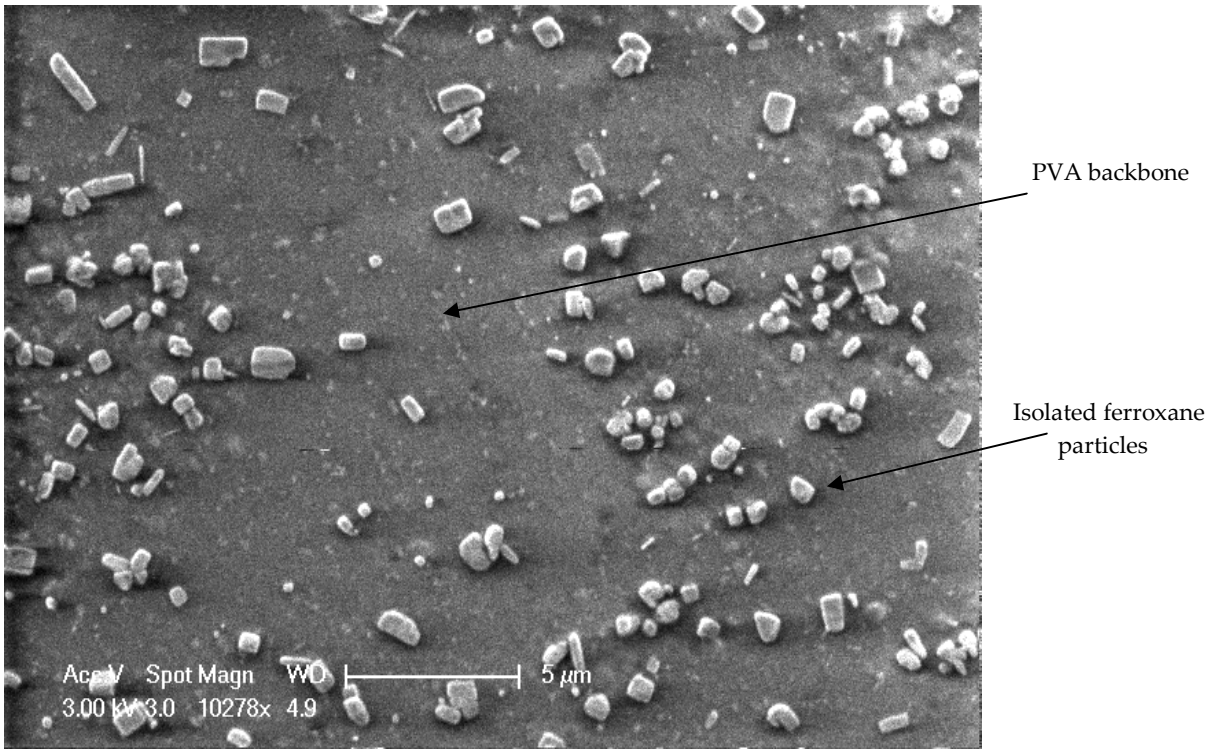

Figure 28: SEM image of the surface of ferroxane-PVA composite membrane

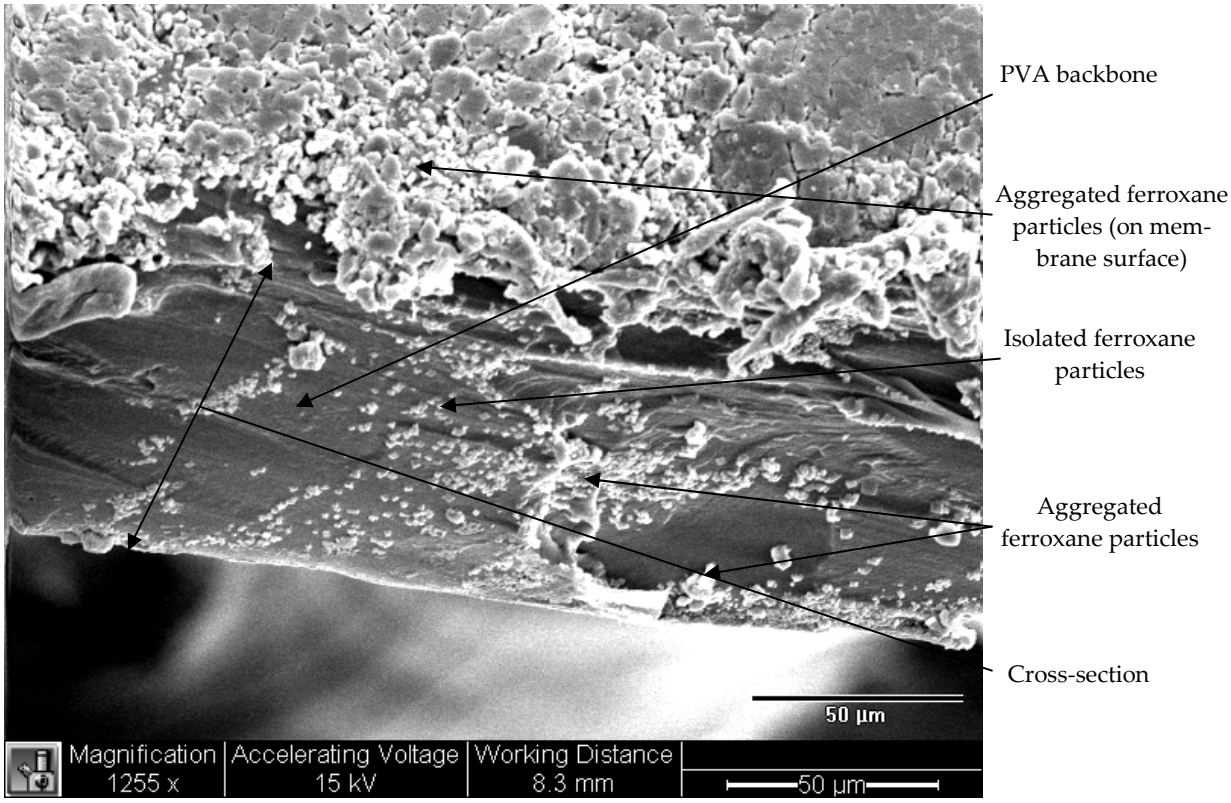

Figure 29: SEM image of the cross-section of the ferroxane-PVA composite membrane. In this image, a large amount of ferroxane particles cluster on the surface of the membrane and the aggregation is very significant, which is quite different from the image of membrane surface (figure 28). Considering the fact that figure 28 and 29 display different parts of the same sample, we can draw a conclusion that the ferroxane nanoparticles are not homogeneously distributed on both the surface and the inner space of the membrane.

4.4 Tensile resistance measurement

The stress-strain curves of ferroxane-PVA composite membranes, pure PVA and Nafion are shown in Figure 30 and the mean values of ultimate breaking strength (σ_B), ultimate breaking strain (ε_B) and tensile modulus (E) of membrane samples are listed in Table 2. It is clear that Fe-PVA composite membranes had larger ultimate breaking strength than the Nafion membrane, which represents that the composite

membranes possess a stronger tensile resistance than Nafion. Furthermore, a higher content of ferroxane in the ferroxane-PVA composite membrane resulted in a stronger tensile resistance. This result can be explained by the formation of Fe-O-CH_2 bonds (this is a hypothesis and needs to be verified by experiments) in Fe-PVA composite membranes. The existence of Fe-O-CH_2 bonds tended to shift the properties of organic polymer material to inorganic material, which led to an increase of resistance to tensile force (high σ_B) but also resulted in a decrease of elasticity (low ε_B). However, the elasticity of the composite membrane with highest ferroxane content (PVA:Fe = 1:4, ε_B = 0.381) was still comparable to that of Nafion membrane (ε_B = 0.417).

The content of ferroxane in the composite membrane also helped to reinforce the stiffness of the membrane (value of *E* (PVA) was only 120 MPa, but values of *E* (ferroxane-PVA samples) were much higher, with a value of 670 MPa for the sample with PVA:Fe = 1:1.5 and 649 MPa for the sample with PVA:Fe = 1:4). The stiffness of Nafion membrane was quite low (*E* = 100 MPa) and was not comparable to that of ferroxane-PVA composite membranes. In summary, ferroxane-PVA composite membranes have better mechanical properties than Nafion membrane.

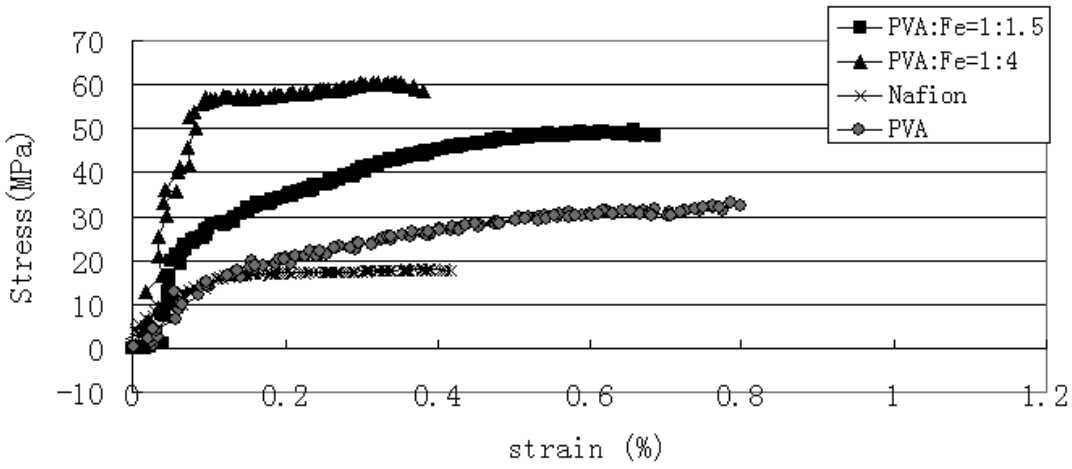

Figure 30: Stress-strain curves of composite membrane samples. ■=composite membrane with a PVA:ferroxane mass ratio of 1:1.5; ▲=composite membrane with a PVA:ferroxane mass ratio of 1:4; ×=Nafion membrane; ●=pure PVA membrane.

Table 2: Tensile resistance parameters of ferroxane-PVA composite membrane samples, Nafion and pure PVA

Sample	σ_B (MPa)	ε_B	E (MPa)
PVA:Fe 1:1.5	49.56	0.683	670.17
PVA:Fe 1:4	60.56	0.381	649.07
Nafion	18.02	0.417	100.35
PVA	32.53	0.798	120

5. Conclusions and future work

FeOOH nanoparticles were shown to produce membranes with higher proton conductivity than did CoOOH nanoparticles. This result is explained by the differences in hydrophilicity of FeOOH and CoOOH. Samples treated by sonication tend to have high proton conductivities at moderate and high RHs (above 81%), and samples treated by reaction with acetic acid + calcination tend to have high proton conductivities at all RHs. Samples treated only by reaction with acetic acid have lower conductivities than sonication-treated and acetic acid + calcination-treated samples, due to the introduction of acetic acid groups to the surfaces of samples. The comparison between proton conductivities of metal oxyhydroxide nanoparticles and proton conductivity of Nafion suggests that FeOOH treated by reaction with acetic acid + calcination had higher proton conductivities (above 0.01 S/cm) than those of Nafion at all RH ranges (33%--100%). FeOOH treated by sonication had proton conductivities higher than those of Nafion at relatively high RHs (above 80%) and CoOOH treated by acetic acid + calcination had proton conductivity higher than Nafion at very low RH (33%).

Based on the conductivity results of metal oxyhydroxide nanoparticles treated by different size-reducing methods, the composite membrane with PVA + FeOOH treated by reaction with acetic acid + calcination is expected to have best proton-conductive performance. Unfortunately, the experimental results showed that the

FeOOH particles treated by reaction with acetic acid + calcination did not dissolve in the PVA solution during the synthesis process of the composite membrane. Therefore, it is impossible to produce a composite membrane with the FeOOH nanoparticles prepared by reaction with acetic acid + calcination homogeneously distributed in the membrane. The composite membrane with sonication-treated FeOOH fillers had very high proton conductivities at relatively high RHs (above 80%), which are higher than those of Nafion and the composite membrane with FeOOH treated only by acetic acid. Therefore, the composite membrane with sonication-treated FeOOH would appear to be the best candidate among all of the Fe-PVA composite membranes to be applied in a PEMFC at high RHs. In the aspect of mechanical strength, the Fe-PVA composite membrane had better mechanical properties than both iron oxyhydroxide ceramics and Nafion membrane, with no brittleness and very high tensile force resistance. However, all Fe-PVA composite membranes had very low proton conductivities (much lower than Nafion) at low RHs (lower than 60%), which partially results from the aggregation of iron oxyhydroxide nanoparticles in the composite membrane (revealed by the SEM images of the ferroxane-PVA composite membrane). Co-PVA composite membranes had low proton conductivities at all RH ranges and did not show promising properties to be applied in practical PEMFC systems.

The proton conductivities of Fe-polysulfone and Co-polysulfone composite membranes were quite low. As a result, these membranes can not meet the

requirement of high proton conductivity and can not be applied in real PEMFC systems. ATR-FTIR spectra of all polysulfone-based composite membranes were almost the same as that of pure polysulfone, which implies that few metal oxyhydroxide nanoparticles are exposed to the surfaces of the composite membranes and that can result in low proton conductivities of the composite membranes.

The shapes of the ATR-FTIR spectra of FeOOH and CoOOH nanoparticles were very similar, which show similar energy absorption behaviors of bonds existing in FeOOH and CoOOH crystals. For FeOOH samples, reaction with acetic acid decreased the absorption band at 2900 cm^{-1}, which can be interpreted as a result of the substitution of -OH groups with CH_3COO- groups during the reaction. However, for CoOOH samples reacted with acetic acid, the decrease of the absorption band at 2900 cm^{-1} was not significant. Moreover, for all samples tested, the introduction of acetic acid groups did not significantly increase the absorption band at 1610 cm^{-1} (characteristic absorption wavenumber of double bonds). Last but not least, the spectra of FeOOH + PVA composite membrane and pure PVA were quite different at the wavenumber of 2900 cm^{-1} (the absorption band of FeOOH + PVA composite at 2900 cm^{-1} was more significant than that of pure PVA), which illustrates a high portion of FeOOH nanoparticles on the surface of the composite. As to CoOOH + PVA composite, the spectra of CoOOH + PVA composite and pure PVA were almost the same, which illustrates a low portion of CoOOH nanoparticles on the surface of the composite. In

summary, the Fe-PVA composite membrane has higher proton conductivity than that of Co-PVA composite, due to the fact that a higher portion of FeOOH nanoparticles are distributed on the surface of Fe-PVA composite and the proton conductivity of FeOOH is higher than that of CoOOH.

Though the proton conductivity test of the composite membranes has illustrated that some composite membrane samples have high proton conductivities at moderate and high RHs and have potentials to be applied in PEMFC systems, the performance of these membranes in real PEMFC systems has not been tested. Therefore, future work of this research in short term will mainly involve the in-situ performance test of proton-conductive composite membrane samples in real PEMFC systems and the optimization of operating parameters (temperature, flow rates of oxygen and hydrogen, etc).

As mentioned in previous sections, the biggest problem for the iron-based composite membranes is their low proton conductivities at low RHs. Therefore, future work of this research in long term will focus on the exploration of possible approaches to improve the proton conductivities of the composites at low RHs. Firstly, the development of appropriate selection methodology to pick polymers that are compatible with metal oxyhydroxide fillers without doing experimental tests is important. Until now, researchers can not predict the proton conductivity of a composite membrane without doing experimental tests. They can only synthesize

composite membrane samples first, and then test the proton conductivities of the samples. That is to say, to find a suitable polymer requires the trial of polymers one by one from a pool with tens of thousands of polymers available. If a prediction approach can be developed and the proton conductivity of a composite membrane can be predicted given the properties of the polymer used, lots of labors and time can be saved. Therefore, the development of reliable selection methodology to pick polymers will be a great breakthrough in the research to synthesize proton-conductive composite membranes. To achieve the goal of proton conductivity prediction without experimental measurement of the membrane sample, an in-depth understanding of complex interactions between proton-conductive nanoparticles and polymer matrix is necessary. Secondly, feasible approaches need to be developed to prevent the aggregation of nanoparticle fillers during the preparation process of the composite membrane, because the aggregation of nanoparticle fillers can reduce the active surface area of the fillers very significantly. The aggregation of nanoparticle fillers is likely to occur during the solvent dried-out process, where the static condition is favorable for the nanoparticles to aggregate. To process the volatilization of solvent in a sonication bath may be a workable method to provide a "stirring" condition, so as to prevent the nanoparticle fillers from aggregation. Thirdly, the exploration of new proton-conductive metal oxyhydroxide nanoparticles (metal oxyhydroxides with metal elements close to iron in the periodic table are worth a try) may contribute to the

development of new composite membranes with higher proton conductivities. Last but not least, based on the fact that ferroxane sintered at 300℃ has a much higher protonic conductivity than ferroxane green body, to find heat-resistant polymers that enable the composite membrane to experience high-temperature sintering may result in the synthesis of composite membrane with high proton conductivity. All possible approaches mentioned to increase the protonic conductivity of the composite membrane are summarized in figure 31.

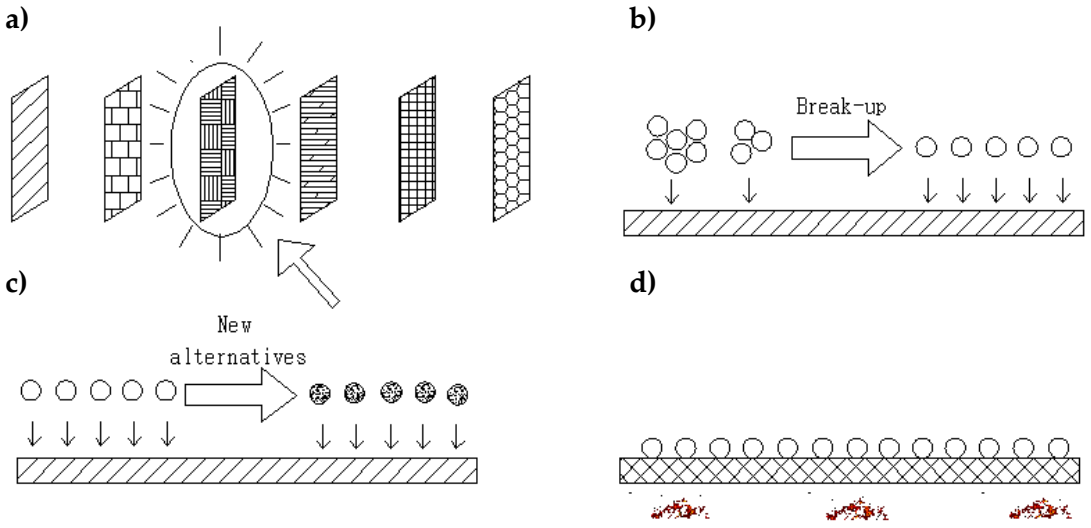

Figure 31: Schematic view of possible approaches to increase the protonic conductivity of the composite membrane. a) Development of selection methodology for quick pick-up of workable polymers. b) Development of approaches to prevent nanoparticles from aggregation during the preparation process. c) Exploration of new metal oxyhydroxide nanoparticles that may possess high protonic conductivity; d) Synthesis of composite membrane that can endure high-temperature sintering.

Another issue that needs to be investigated in future is the possible transformation of FeOOH or ferroxane in the composite membrane into other iron oxide phases during the operation of fuel cell. That investigation is quite necessary because if FeOOH or ferroxane experiences unwanted reactions during the operation of fuel cell, the products may cause fouling of the membrane and abatement of water molecules adsorbed on the surface of the membrane, thus result in a deterioration of the performance of the fuel cell. To the best of my knowledge, ferroxane is quite stable under normal conditions, but a loss of acetic acid groups from the surface of the material can occur at high temperature and the material can be transformed into FeOOH [18]. This reaction is favorable for proton conduction, so it will not raise much concern on the performance deterioration of the membrane.

FeOOH may also experience phase change reactions during the operation of fuel cell and most products have less water--adsorption capacity, compared with pure FeOOH. One major transformation reaction of FeOOH is dehydration reaction, which can occur under the influence of either heat or mechanical stress [31]:

$$2FeOOH \rightarrow Fe_2O_3 + 2H_2O$$

The end product of the FeOOH dehydration reaction is hematite and maghemite is generated as an intermediate form [31]. Fe_2O_3 has no hydroxyl groups on its surface, which makes it difficult to attract water molecules and conduct protons. This reaction may take place at a wide range of temperature (140--500℃) [31], therefore,

if acetic acid + sintering method is applied to prepare FeOOH nanoparticles, a partial phase change of FeOOH to Fe_2O_3 may occur during the preparation process. Moreover, mechanical stress, such as grinding, can also lead to a partial conversion of FeOOH to maghemite and hematite [70]. As the membrane containing FeOOH is compressed tightly by two electrodes in the fuel cell, some mechanochemical conversion of FeOOH may occur.

The exposure of FeOOH to H^+ in the fuel cell may lead to so-called protonation reaction [31, 70]:

$$FeOOH + nH^+ \rightarrow [Fe(OH)_{(3-n)}]^{n+} + (n-1)H_2O$$

This reaction requires an environment with high water content; therefore, the cathode side of the fuel cell is an ideal place for the protonation reaction to occur (water is produced as an end product at the cathode side). The reaction results in the release of free Fe (III) ions and the crystal structure of FeOOH may be destroyed if the protonation reaction is processed at a high rate. Therefore, water produced at the cathode side needs to be emitted from the system continuously and the lifetime of the composite membrane when installed in the fuel cell needs to be investigated, especially when the fuel cell is operated in a humid environment.

There is flow of free electrons from anode to cathode in the fuel cell and the iron oxyhydroxide phase in the composite membrane is exposed to the free electrons.

These electrons, associated with Fe (III) ions produced from protonation reaction, can lead to the reduction of FeOOH to magnetite [31]:

$$2FeOOH + Fe^{3+} + e^{-} \longrightarrow Fe_3O_4 + 2H^{+}$$

Note that this reaction can produce H^{+}, which can promote the protonation reaction.

In summary, a series of chemical reactions may occur if FeOOH is the inorganic content in the composite PEM for fuel cell applications and the effect of these reactions on the performance of the membrane during the operation of fuel cell is not well studied. If the integration of these reactions can lead to a significant composition change of the iron oxyhydroxide phase in the composite membrane, the proton conductivity results obtained in my EIS experiments will not reflect the in-situ performance of the membrane in fuel cell. Therefore, the conversion of FeOOH phase to other iron oxide phases in the composite PEM during the operation period of fuel cell needs to be well studied in future, with the use of X-ray diffraction or other characterization techniques that can distinguish the structural variance of different iron oxide phases.

References

1. Hoogers, G., *Fuel cell technology handbook*. 2003, Boca Raton, Fla.: CRC Press. 1 v. (various pagings).

2. Smitha, B., S. Sridhar, and A.A. Khan, *Solid polymer electrolyte membranes for fuel cell applications - a review.* Journal of Membrane Science, 2005. **259**(1-2): p. 10-26.

3. Zaidi, J., *Polymer membranes for fuel cells*. 2008, New York: Springer.

4. Sammes, N.M., *Fuel cell technology : reaching towards commercialization*. Engineering materials and processes. 2006, London: Springer. xiv, 298 p.

5. Berger, C., *Handbook of fuel cell technology*. 1968, Englewood Cliffs, N.J.,: Prentice-Hall. xv, 607 p.

6. Turner, W.C. and S. Doty, *Energy management handbook*. 6th ed. 2007, Lilburn, GA Boca Raton, FL: Fairmont Press; Distributed by CRC Press/Taylor & Francis. xiii, 909 p.

7. Dicks, A.L., *Molten carbonate fuel cells.* Current Opinion in Solid State & Materials Science, 2004. **8**(5): p. 379-383.

8. Watanabe, M., et al., *Activity and Stability of Ordered and Disordered Co-Pt Alloys for Phosphoric-Acid Fuel-Cells.* Journal of the Electrochemical Society, 1994. **141**(10): p. 2659-2668.

9. McLean, G.F., et al., *An assessment of alkaline fuel cell technology.* International Journal of Hydrogen Energy, 2002. **27**(5): p. 507-526.

10. Steele, B.C.H. and A. Heinzel, *Materials for fuel-cell technologies.* Nature, 2001. **414**(6861): p. 345-352.

11. Hickner, M.A., et al., *Alternative polymer systems for proton exchange membranes (PEMs).* Chemical Reviews, 2004. **104**(10): p. 4587-4611.

12. Schmidt-Rohr, K. and Q. Chen, *Parallel cylindrical water nanochannels in Nafion fuel-cell membranes.* Nature Materials, 2008. **7**(1): p. 75-83.

13. Zawodzinski, T.A., et al., *A Comparative-Study of Water-Uptake by and Transport through Ionomeric Fuel-Cell Membranes.* Journal of the Electrochemical Society, 1993. **140**(7): p. 1981-1985.

14. Motupally, S., A.J. Becker, and J.W. Weidner, *Diffusion of water in Nafion 115 membranes.* Journal of the Electrochemical Society, 2000. **147**(9): p. 3171-3177.

15. Schlick, S., *Ionomers : characterization, theory, and applications*. 1996, Boca Raton: CRC Press. 311 p.

16. Eisenberg, A., H.L. Yeager, and American Chemical Society. Division of Polymer Chemistry., *Perfluorinated ionomer membranes : developed in advance of the Polymer Division topical workshop on per-fluorinated ionomer membranes, Lake Buena Vista, Florida, February 23-26, 1982*. ACS symposium series. 1982, Washington, D.C.: American Chemical Society. ix, 500 p.

17. Casciola, M., et al., *On the decay of Nafion proton conductivity at high temperature and relative humidity.* Journal of Power Sources, 2006. **162**(1): p. 141-145.

18. Tsui, E.M., M.M. Cortalezzi, and M.R. Wiesner, *Proton conductivity and methanol rejection by ceramic membranes derived from ferroxane and alumoxane precursors.* Journal of Membrane Science, 2007. **306**(1-2): p. 8-15.

19. Elabd, Y.A., et al., *Triblock copolymer ionomer membranes Part I. Methanol and proton transport.* Journal of Membrane Science, 2003. **217**(1-2): p. 227-242.

20. Kim, Y.S., et al., *Sulfonated poly(arylene ether sulfone) copolymer proton exchange membranes: composition and morphology effects on the methanol permeability.* Journal of Membrane Science, 2004. **243**(1-2): p. 317-326.

21. Mukoma, P., B.R. Jooste, and H.C.M. Vosloo, *A comparison of methanol permeability in Chitosan and Nafion 117 membranes at high to medium methanol concentrations.* Journal of Membrane Science, 2004. **243**(1-2): p. 293-299.

22. Vichi, F.M., M.T. Colomer, and M.A. Anderson, *Nanopore ceramic membranes as novel electrolytes for proton exchange membranes.* Electrochemical and Solid State Letters, 1999. **2**(7): p. 313-316.

23. Vichi, F.M., M.I. Tejedor-Tejedor, and M.A. Anderson, *Effect of pore-wall chemistry on proton conductivity in mesoporous titanium dioxide.* Chemistry of Materials, 2000. **12**(6): p. 1762-1770.

24. Tsui, E.M. and M.R. Wiesner, *Fast proton-conducting ceramic membranes derived from ferroxane nanoparticle-precursors as fuel cell electrolytes.* Journal of Membrane Science, 2008. **318**(1-2): p. 79-83.

25. Xu, W., et al., *Low methanol permeable composite Nafion/silica/PWA membranes for low temperature direct methanol fuel cells.* Electrochimica Acta, 2005. **50**(16-17): p. 3280-3285.

26. Anderson, J.H. and G.A. Parks, *Electrical Conductivity of Silica Gel in Presence of Adsorbed Water.* Journal of Physical Chemistry, 1968. **72**(10): p. 3662-&.

27. Park, S.M. and J.S. Yoo, *Electrochemical impedance spectroscopy for better electrochemical measurements.* Analytical Chemistry, 2003. **75**(21): p. 455a-461a.

28. Ernsberger, F.M., *The Non-Conformist Ion.* Journal of the American Ceramic Society, 1983. **66**(11): p. 747-750.

29. Sun, H.T., et al., *Porosity Control of Humidity-Sensitive Ceramics and Theoretical-Model of Humidity-Sensitive Characteristics.* Sensors and Actuators, 1989. **19**(1): p. 61-70.

30. Traversa, E., *Ceramic Sensors for Humidity Detection - the State-of-the-Art and Future-Developments.* Sensors and Actuators B-Chemical, 1995. **23**(2-3): p. 135-156.

31. Cornell, R.M. and U. Schwertmann, *The iron oxides : structure, properties, reactions, occurrences, and uses*. 2nd, completely rev. and extended ed. 2003, Weinheim: Wiley-VCH. xxxix, 664 p.

32. Dutch S., *Lepidocrocite and Boehmite Structure,* [on-line webpage]. URL: http://www.uwgb.edu/dutchs/Petrology/LepidocrStruc.HTM.

33. Kickelbick, G., *Hybrid materials : synthesis, characterization, and applications*. 2007, Weinheim: Wiley - VCH. xvii, 498 p.

34. Gao, F.M., et al., *Hardness of covalent crystals.* Physical Review Letters, 2003. **91**(1): p. -.

35. Ishikawa, T., N. Kodaira, and K. Kandori, *Step-Like Adsorption-Isotherms of Molecules on Gamma-Feooh and the Surface Homogeneity of Gamma-Feooh.* Journal of the Chemical Society-Faraday Transactions, 1992. **88**(5): p. 719-722.

36. Schottner, G., *Hybrid sol-gel-derived polymers: Applications of multifunctional materials.* Chemistry of Materials, 2001. **13**(10): p. 3422-3435.

37. Riken Research, *Using Metamaterials to Defy Our Common Understanding of Light* [on-line webpage].URL: http://www.rikenresearch.riken.jp/eng/frontline/5930.

38. Materials Science and Engineering Portal, *Mesoporous Silica* [on-line webpage].URL: http://en.wikipedia.org/wiki/File:Mesoporous_silica_SEM.jpg

39. UW Chemical Engineering Department, *Research area of Dr. Dumesic* [on-line webpage]. URL: http://jamesadumesic.che.wisc.edu/research.htm

40. Kim, Y.S., et al., *Fabrication and characterization of heteropolyacid (H3PW12O40)/directly polymerized sulfonated poly(arylene ether sulfone) copolymer composite membranes for higher temperature fuel cell applications.* Journal of Membrane Science, 2003. **212**(1-2): p. 263-282.

41. Genova-Dimitrova, P., et al., *Ionomeric membranes for proton exchange membrane fuel cell (PEMFC): sulfonated polysulfone associated with phosphatoantimonic acid.* Journal of Membrane Science, 2001. **185**(1): p. 59-71.

42. Refait, P. and J.M.R. Genin, *The Oxidation of Ferrous Hydroxide in Chloride-Containing Aqueous-Media and Pourbaix Diagrams of Green Rust One.* Corrosion Science, 1993. **34**(5): p. 797-819.

43. Rose, J., et al., *Synthesis and characterization of carboxylate-FeOOH nanoparticles (ferroxanes) and ferroxane-derived ceramics.* Chemistry of Materials, 2002. **14**(2): p. 621-628.

44. Mineralogy Database, *Heterogenite-3R Mineral Data* [on-line webpage]. URL: http://webmineral.com/data/Heterogenite-3R.shtml

45. Sakurada, I., *Polyvinyl alcohol fibers*. International fiber science and technology series. 1985, New York: M. Dekker. xiii, 449 p.

46. Mbhele, Z.H., et al., *Fabrication and characterization of silver-polyvinyl alcohol nanocomposites.* Chemistry of Materials, 2003. **15**(26): p. 5019-5024.

47. Qian, X.F., et al., *The preparation and characterization of PVA/Ag2S nanocomposite.* Materials Chemistry and Physics, 2001. **68**(1-3): p. 95-97.

48. Kumar, R.V., et al., *Sonochemical preparation and characterization of nanocrystalline copper oxide embedded in poly(vinyl alcohol) and its effect on crystal growth of copper oxide.* Langmuir, 2001. **17**(5): p. 1406-1410.

49. Kumar, R.V., et al., *Preparation of amorphous magnetite nanoparticles embedded in polyvinyl alcohol using ultrasound radiation.* Journal of Materials Chemistry, 2000. **10**(5): p. 1125-1129.

50. Strawhecker, K.E. and E. Manias, *Structure and properties of poly(vinyl alcohol)/Na+ montmorillonite nanocomposites.* Chemistry of Materials, 2000. **12**(10): p. 2943-2949.

51. Nexant Chemical Systems, *PERP Program--New Report Alert (March 2005)* [on-line webpage]. URL: http://chemsystems.com/reports/search/docs/abstracts/0304-S12-abs.pdf

52. O'Hayre, R.P., *Fuel cell fundamentals*. 2006, Hoboken, NJ: John Wiley & Sons. xxii, 409 p.

53. Lee, C.H., et al., *Importance of proton conductivity measurement in polymer electrolyte membrane for fuel cell application.* Industrial & Engineering Chemistry Research, 2005. **44**(20): p. 7617-7626.

54. Somasundaran, P., *Encyclopedia of surface and colloid science*. 2nd ed. 2006, New York: Taylor & Francis.

55. Doran, E.M., M.G. Yost, and R.A. Fenske, *Measuring dermal exposure to pesticide residues with attenuated total reflectance Fourier transform infrared (ATR-FTIR) spectroscopy.* Bulletin of Environmental Contamination and Toxicology, 2000. **64**(5): p. 666-672.

56. Bart, J.C.J., *Plastics additives : advanced industrial analysis*. 2006, Amsterdam ; Washington, DC: IOS Press. xv, 808 p.

57. Dunuwila, D.D. and K.A. Berglund, *ATR FTIR spectroscopy for in situ measurement of supersaturation.* Journal of Crystal Growth, 1997. **179**(1-2): p. 185-193.

58. PerkinElmer Life and Analytical Sciences, *FT-IR Spectroscopy Attenuated Total Reflectance (ATR).* Technical note, 2005 [on-line webpage]. URL: www.perkinelmer.com

59. Flegler, S.L., J.W. Heckman, and K.L. Klomparens, *Scanning and transmission electron microscopy : an introduction*. 1993, New York: W.H. Freeman. viii, 225 p.

60. Department of radiological and environmental management, Purdue University, *Scanning electron microscope (SEM)* [on-line webpage]. URL: www.purdue.edu/REM/rs/sem.htm

61. Gere, J.M., *Mechanics of materials*. 6th ed. 2004, Belmont, CA: Brooks/Cole-Thomas Learning. xx, 940 p.

62. Geng, B.Y., et al., *Facile production of self-assembly hierarchical dumbbell-like CoOOH nanostructures and their room-temperature CO-gas-sensing properties.* Crystal Growth & Design, 2008. **8**(10): p. 3497-3500.

63. Hosono, E., et al., *Synthesis of the CoOOH fine nanoflake film with the high rate capacitance property (vol 158, pg 779, 2006).* Journal of Power Sources, 2006. **160**(1): p. 764-764.

64. Casey, W.H. and H.R. Westrich, *Control of Dissolution Rates of Orthosilicate Minerals by Divalent Metal Oxygen Bonds.* Nature, 1992. **355**(6356): p. 157-159.

65. Tubbs, R.K., *Melting Point and Heat of Fusion of Poly(Vinyl Alcohol).* Journal of Polymer Science Part a-General Papers, 1965. **3**(12PA): p. 4181-&.

66. Antony, H., et al., *Electrochemical synthesis of lepidocrocite thin films on gold substrate - EQCM, IRRAS, SEM and XRD study.* Electrochimica Acta, 2004. **50**(4): p. 1015-1021.

67. Cudennec, Y. and A. Lecerf, *Structural comparison between Cu(OH)(2(s)) and gamma- FeO(OH)((s)).* Comptes Rendus De L Academie Des Sciences Serie Ii Fascicule C-Chimie, 2001. **4**(12): p. 885-891.

68. Costa, V.C., et al., *Preparation of hybrid biomaterials for bone tissue engineering.* Materials Research, 2007. **10**: p. 21-26.

69. Belfer, S., et al., *Surface characterization by FTIR-ATR spectroscopy of polyethersulfone membranes-unmodified, modified and protein fouled.* Journal of Membrane Science, 2000. **172**(1-2): p. 113-124.

70. Gomezvillacieros, R., et al., *Mechanochemical Preparation and Thermal-Stability of Gamma-Fe_2O_3 Derived from Gamma-Feooh.* Materials Research Bulletin, 1987. **22**(4): p. 513-520.